Electronic Supporting Information

# A molecular sheaf: doubly threaded [6]rotaxane

Song Huang,[a] Zhenwen Wang,[a] Jinyang Wu,[a] Xinyan Mai,[a] Song Qin,[a] Yuqiao Zhou,[a] Daqiang Yuan,[b] Xiaowei Li,*[, a] Wen Feng[a] and Lihua Yuan*[, a]

[a] College of Chemistry, Key Laboratory of Radiation Physics and Technology of Ministry of Education, Institute of Nuclear Science and Technology, Sichuan University, Chengdu, 610064, China

[b] State Key Laboratory of Structural Chemistry, Fujian Institute of Research on the Structure of Matter, Chinese Academy of Sciences, Fuzhou, 350002, China

E-mail: lhyuan@scu.edu.cn, lixw@scu.edu.cn

# Contents

# 1. Materials and Methods

All chemicals were obtained from commercial suppliers and were used as received unless other-wise noted. Solvents were dried and distilled following usual protocols. Solvents for NMR were purchased from Cambridge Isotope Laboratories (CIL). Analytical NMR spectra were recorded on Bruker AVANCE AV II-400/600 MHz at room temperature of 298 K ($^1$H: 400 MHz, 600 MHz; 2D: 600 MHz). Chemical shifts are reported in δ values in ppm using tetramethylsilane (TMS) or residual solvent as internal standard and coupling constants (J) are denoted in Hz. Multiplicities are denoted as follows: s = singlet, d = doublet, t = triplet, dd = double doublet and m = multiplet. Electrospray ionization high resolution mass (ESI-HRMS) data were collected by WATERS Q-TOF Premier. UV-vis spectra were measured by SHIMADZU UV-2450. Single crystal X-ray data were measured on a Xcalibur E diffractometer with graphite monochromated Cu-Kα radiation (λ=1.54184 Å). Data collection and structure refinement details can be found in the CIF files or obtained free of charge via *https://www.ccdc.cam.ac.uk/*. Isothermal titration calorimetry (ITC) was performed on a TA NANO-ITC Microcalorimeter with Origin 7 software.

# 2. Synthesis

## 2.1 Synthesis of Host 1a

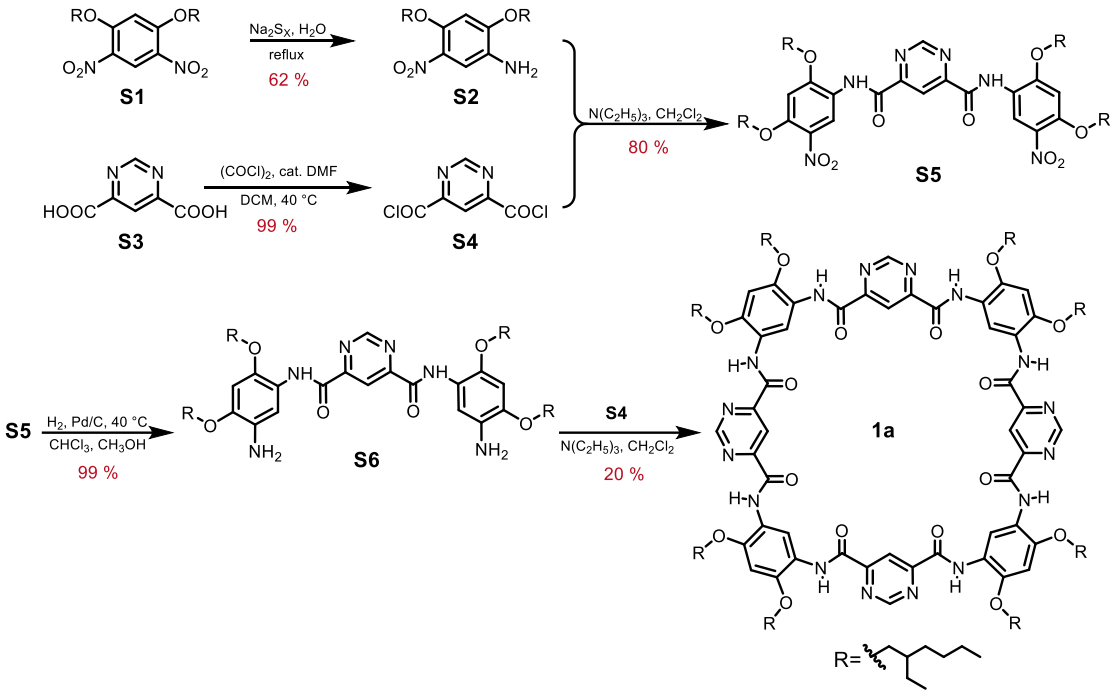


**Scheme S1** Synthetic route of **1a**.

**1a** was prepared according to literature procedures.[1]

**S2:** The reducing agent, i.e., $Na_2S_x$ solution, was freshly prepared before use. Briefly, sulfur powder (6.28 g, 0.20 mol) was mixed with $Na_2S{\cdot}9H_2O$ (25.2 g, 0.10 mol) and water (2 mL). The mixture was stirred under reflux at 100 °C, during which the initially colorless solution gradually turned into a dark red solution. After the sulfur powder was completely dissolved, the stirring and heating were kept for another 30 min to obtain a dark red $Na_2S_x$ solution. After a solution of **S1** (5.11 g, 9.08 mmol) in ethanol (10 mL) was heated to 80 °C, the freshly prepared $Na_2S_x$ solution was added dropwise. The mixture was refluxed for 10 h and cooled down to room temperature. The mixture was diluted with water (100 mL) and extracted with ethyl acetate (3 × 50 mL). The combined organic extracts were dried over anhydrous sodium sulfate and filtered. After removal of the solvent, the residue was chromatographed on a silica gel column using a mixture of petroleum ether and $CH_2Cl_2$ (from 1:1 to 1:5, v/v) as the eluent. A brown oil was obtained (2.95 g, 62%). $^1$H NMR (400 MHz, $CDCl_3$), δ 7.38 (s, 1H), 6.46 (s, 1H), 3.94 (ddd, J = 12.1, 5.6, 1.8 Hz, 4H), 3.72 (s, 2H), 1.85 - 1.72 (m, 2H), 1.62 - 1.41 (m, 8H), 1.33 (dh, J = 7.3, 3.9 Hz, 8H), 0.93 (tt, J = 10.5, 7.2 Hz, 12H).

**S4:** The pyrimidine-4,6-dicarbonyl chloride **S4** was freshly prepared before use. To a suspension solution of pyrimidine-4,6-dicarboxylic acid **S3** (1.68 g, 10.0 mmol) in anhydrous $CH_2Cl_2$ (50 mL), oxalyl chloride (3.81 g, 30.0 mmol) was added. After one drop of dimethyl formamide (10 μL) was added, the mixture was stirred under reflux for 4 h. The progress of the reaction was monitored by TLC (developing solvent: ethyl acetate). The solvent and residual oxalyl chloride was then removed under vacuum to afford **S4** as a grey powder. The product was directly used for the next step without further purification.

**S5:** To a mixture of **S2** (8.67 g, 22.0 mmol) and dry triethylamine (2.92 g, 28.9 mmol) in anhydrous $CH_2Cl_2$ (80 mL) was added dropwise a freshly prepared solution of pyrimidine-4,6-dicarbonyl chloride **S4** in anhydrous $CH_2Cl_2$ (50 mL). The mixture was stirred for 5 h under $N_2$ atmosphere. After the organic solvent was removed under reduced pressure, the residue was extracted with methanol and ethyl acetate by solid-liquid extraction, successively, and the filtered residue was collected. A yellow floccose solid was obtained (4.39 g, 80%). $^1$H NMR (400 MHz, $CDCl_3$) δ 10.41 (s, 2H), 9.22 (s, 2H), 6.58 (s, 2H), 4.12 (d, J = 5.4 Hz, 4H), 4.00 (dd, J = 5.6, 1.7 Hz, 4H), 1.94 (h, J = 6.1 Hz, 2H), 1.81 (h, J = 6.1 Hz, 2H).

**S6:** Compound **S5** (1.04 g, 1.14 mmol) was hydrogenated in the presence of 10% Pd/C (300 mg) in the solvent of $CHCl_3$/$CH_3OH$ (80 mL, 3:1, v/v) for 10 h at 40 °C. The solution was filtered in darkness as quickly as possible followed by immediate removal of the solvent to afford the diamine **S6**. The obtained product was used directly for the next step without further purification.

**1a:** To the flask of compound **S6**, anhydrous $CH_2Cl_2$ (300 mL) and dry triethylamine (362 mg, 3.58 mmol) were added. Then the solution was stirred for 10 minutes, an anhydrous $CH_2Cl_2$ solution (40 mL) of **S4**, which was freshly prepared from **S3** (200 mg, 1.20 mmol), was added dropwise. The resulting mixture was stirred for 10 h under $N_2$ atmosphere and quenched by $CH_3OH$ (2 mL). After removal of the solvent, the residue was triturated with $CH_3OH$, ethyl acetate and tetrahydrofuran, successively. The remaining residue was filtered and collected to afford the desired product **1a** as a yellow powder (226 mg, 20%). $^1$H NMR (400 MHz, $CDCl_3$) δ 10.23 (s, 4H), 10.08 (s, 8H), 9.40 (d, J = 1.3 Hz, 4H), 9.27 (d, J = 1.3 Hz, 4H), 6.59 (s, 4H), 4.01 (d, J = 5.5 Hz, 16H), 1.88 (p, J = 5.9 Hz, 8H), 1.70 - 1.50 (m, 55H), 1.41 (ddt, J = 10.9, 6.9, 4.3 Hz, 36H), 1.04 (t, J = 7.5 Hz, 26H), 0.94 (t, J = 7.1 Hz, 26H).

## 2.2 Synthesis of Guests G1-G3

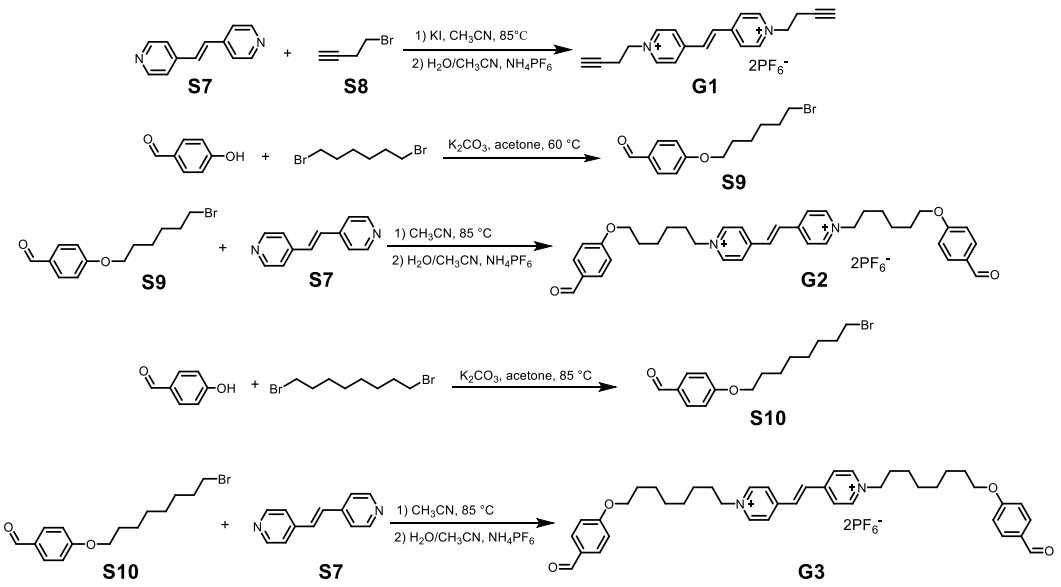


**Scheme S2** Synthetic routes of **G1** and **G2**.

**S9** and **S10** was prepared according to literature procedures.[2]

Guests **G1**-**G3** were prepared according to the similar procedures in the literature.[3]

**S9**: To a round bottom flask equipped with a stir bar was added 4-hydroxylaldehyde (2.50 g, 20.5 mmol), 1,6-dibromohexane (9.5 mL, 61.5 mmol), potassium carbonate (4.80 g, 34.8 mmol), and acetone (45 mL). The round bottom flask was then attached to an air condenser and refluxed at 60 ˚C for 48 h. The reaction was cooled to room temperature and extracted with ethyl acetate (100 mL) and washed with water (30 mL × 3), brine (20 mL × 2). The organic layer was then dried over sodium sulfate, filtered, and concentrated under vacuum. The crude yellow oil was eluted with a $CH_2Cl_2$/hexane (1:1, v/v) solvent mixture on a silica column to yield **S9** as a white solid (5.40 g, 90%). $^1$H NMR (400 MHz, $CDCl_3$, 298 K) δ 9.89 (d, J = 3.4 Hz, 1H), 7.84 (dd, J = 8.7, 3.2 Hz, 2H), 7.00 (dd, J = 8.9, 2.5 Hz, 2H), 4.06 (td, J = 6.4, 3.2 Hz, 2H), 3.44 (t, J = 6.7 Hz, 2H), 1.97 - 1.79 (m, 4H), 1.52 (d, J = 3.6 Hz, 4H).

**S10**: To a round bottom flask equipped with a stir bar was added 4-hydroxylaldehyde (1.94 g, 16.0 mmol), tetrabutylammonium chloride (360 mg, 1.3 mmol), sodium carbonate (16.80 g, 160 mmol), and acetone (45 mL). The solution was stirred at room temperature for 20 min. After this time, 1,8-dibromooctane (8.8 mL, 48.0 mmol) was added. The round bottom flask was then attached to an air condenser and refluxed at 60 ˚C for 48 h. The reaction was cooled to room temperature and extracted with ethyl acetate (100 mL) and washed with water (30 mL × 3), brine (20 mL × 2). The organic layer was then dried over sodium sulfate, filtered, and concentrated under vacuum. The crude yellow

oil was eluted with a $CH_2Cl_2$/hexane (1:1, v/v) solvent mixture on a silica column to yield **S10** as a white solid (3.00 g, 60%). $^1$H NMR (400 MHz, $CDCl_3$, 298 K) δ 9.88 (s, 1H), 7.83 (d, J = 8.8 Hz, 2H), 6.99 (d, J = 8.7 Hz, 2H), 4.04 (t, J = 6.5 Hz, 2H), 3.41 (t, J = 6.8 Hz, 2H), 1.91-1.77 (m, 4H), 1.53-1.32 (m, 8H).

**G1:** A mixture of trans-1,2-bis(4-pyridyl)ethene **S7** (1.00 g, 5.49 mmol), 4-bromobut-1-yne **S8** (2.92 g, 21.95 mmol) and potassium iodide (0.18 g, 1.10 mmol) was stirred in 20 mL $CH_3CN$ at 80 ˚C for 96 h, and then cooled to room temperature. The pale yellow precipitate was filtered off and washed with $CH_3CN$ (20 mL). The solid was then dissolved in $H_2O$ (15 mL), and a saturated aqueous solution of $NH_4PF_6$ was added until no further precipitation was observed. The precipitate was filtered off and washed with $H_2O$ (30 mL), EtOH (15 mL), and $Et_2O$ (10 mL) to afford **G1** as a light brown solid (1.71 g, 54%). $^1$H NMR (400 MHz, $CD_3CN$, 298 K) δ 8.76 (d, *J* = 6.9 Hz, 4H), 8.22 (d, *J* = 6.9 Hz, 4H), 7.87 (s, 2H), 4.68 (t, *J* = 6.4 Hz, 4H), 2.96 (td, *J* = 6.4, 2.6 Hz, 4H), 2.46 (t, *J* = 2.6 Hz, 2H). $^{13}$C NMR (100 MHz $CD_3CN$, 298 K) δ 150.96, 141.49, 133.34, 123.67, 78.71, 71.80, 59.32, 23.06. ESI-HRMS: m/z calculated for $C_{20}H_{20}F_6N_2P^{2+}$ $[M\text{-}PF_6^-]^+$ 433.1260; found 433.1251.

**G2:** A mixture of trans-1,2-bis(4-pyridyl)ethene **S7** (0.50 g, 2.74 mmol), 4-((6-bromohexyl)oxy)benzaldehyde **S9** (3.13 g, 10.98 mmol) was stirred in 15 mL $CH_3CN$ at 80 ˚C for 96 h, and then cooled to room temperature. The pale yellow precipitate was filtered off and washed with $CH_3CN$ (20 mL). The solid was then dissolved in $H_2O$ (15 mL), and a saturated aqueous solution of $NH_4PF_6$ was added until no further precipitation was observed. The precipitate was filtered off and washed with $H_2O$ (30 mL), EtOH (15 mL), and $Et_2O$ (10 mL) to afford **G2** as a light brown solid (1.45 g, 60%). $^1$H NMR (400 MHz, $CD_3CN$, 298 K) δ 9.87 (s, 2H), 8.70 (d, *J* = 6.9 Hz, 4H), 8.17 (d, *J* = 6.7 Hz, 4H), 7.86 (d, *J* = 8.8 Hz, 4H), 7.81 (s, 2H), 7.07 (d, *J* = 8.8 Hz, 4H), 4.53 (d, *J* = 7.5 Hz, 4H), 4.10 (d, *J* = 6.4 Hz, 4H), 2.04 (p, *J* = 7.5 Hz, 4H), 1.87 - 1.79 (m, 4H), 1.61 - 1.51 (m, 4H), 1.51 - 1.42 (m, 4H). $^{13}$C NMR (100 MHz $CD_3CN$, 298 K) δ 190.92, 164.06, 151.00, 144.76, 133.80, 131.76, 130.01, 125.91, 113.94, 67.61, 61.39, 30.17, 27.68, 25.20, 25.00. ESI-HRMS: m/z calculated for $C_{38}H_{44}N_2O_4^{2+}$ $[M\text{-}2PF_6^-]^{2+}$ 296.1645; found 296.1645.

**G3:** A mixture of trans-1,2-bis(4-pyridyl)ethene **S7** (72.7 mg, 0.40 mmol), 4-((8-bromooctyl)oxy)benzaldehyde **S10** (0.50 g, 1.60 mmol) was stirred in 15 mL $CH_3CN$ at 80 ˚C for 96 h, and then cooled to room temperature. The pale yellow precipitate was filtered off and washed with $CH_3CN$ (20 mL). The solid was then dissolved in $H_2O$ (15 mL), and a saturated aqueous

solution of $NH_4PF_6$ was added until no further precipitation was observed. The precipitate was filtered off and washed with $H_2O$ (30 mL), EtOH (15 mL), and $Et_2O$ (10 mL) to afford **G3** as a white solid (108.8 mg, 42%). $^1$H NMR (400 MHz, $CD_3CN$, 298 K) δ 9.85 (s, 1H), 8.67 (d, J = 6.9 Hz, 2H), 8.15 (d, J = 6.9 Hz, 2H), 7.83 (d, J = 8.8 Hz, 2H), 7.80 (s, 1H), 7.04 (d, J = 8.8 Hz, 2H), 4.50 (t, J = 7.5 Hz, 2H), 4.08 (t, J = 6.5 Hz, 2H), 2.03-1.95 (m, 2H), 1.83-1.72 (m, 2H), 1.50- 1.41 (m, 2H), 1.39 (m, 6H). $^{13}$C NMR (100 MHz, $CD_3CN$, 298 K) δ 190.91, 133.81, 129.97, 61.47, 28.64, 28.62, 28.45, 25.46, 25.42. ESI-HRMS: m/z calculated for $C_{42}H_{52}N_2O_4^{2+}$ $[M\text{-}2PF_6^-]^{2+}$ 324.1958; found 324.1958.

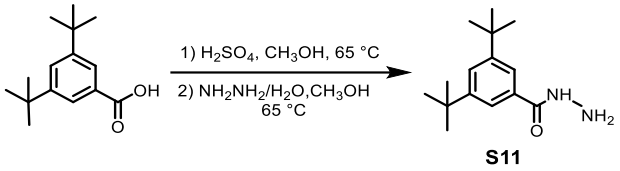


**Scheme S3** Synthetic route of **S11**.

**S11** was prepared according to literature procedures.[4]

**S11**: A mixture of 3,5-di-tert-butylbenzoic acid (2.40 g, 10.2 mmol) and concentrated $H_2SO_4$ (1.6 mL) in $CH_3OH$ (24 mL) were heated at 65 ˚C for 16 hours. The reaction mixture was cooled to room temperature and the solvent was removed under reduced pressure. The crude residue dissolved in ethyl acetate (200 mL) and the organic phase was washed with $H_2O$ (2 × 200 mL). It was then dried ($Na_2SO_4$) and the solvent removed under reduced pressure. The resulting waxy solid was used directly without further purification (assumed quant.). To the crude ester (assumed 10.2 mmol) in $CH_3OH$ (24 mL) was added hydrazine hydrate (12 mL, 64 - 65% in $H_2O$). The reaction mixture was heated at 65 ˚C for 24 hours. The mixture was cooled to room temperature and the solvent removed under reduced pressure. The crude residue was taken up in $CH_2Cl_2$ (100 mL) and washed with $H_2O$ (2 × 200 mL). The organic phase was dried ($Na_2SO_4$) and the solvent removed under reduced pressure. **S11** was recovered as a colorless powder which was used without further purification (1.90 g, 7.70 mmol, 75%). $^1$H NMR (400 MHz, $CDCl_3$, 298K) δ 7.62 (s, 1H), 7.60 (d, *J* = 1.6 Hz, 3H), 4.16 (s, 2H), 1.36 (s, 18H).

## 2.2 Synthesis of [6]Rs and [6]Rc

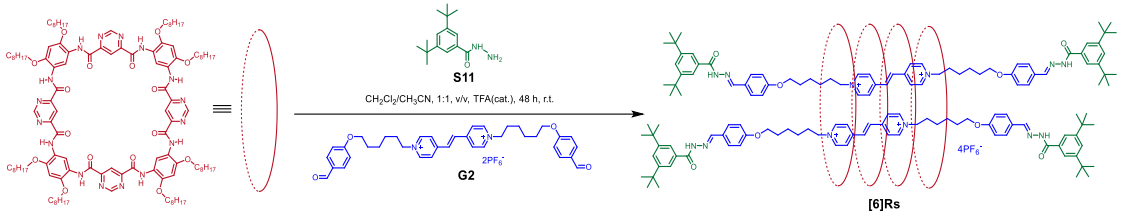


**Scheme S4** Synthetic route of doubly threaded [6]rotaxane **[6]Rs**.

**[6]Rs:** A mixture of macrocycle **1a** (24.8 mg, 12.5 μmol) and guest **G2** (5.00 mg, 5.70 μmol) and was stirred in dry $CH_2Cl_2/CH_3CN$ (1:1, v/v, 18 mL) at room temperature for 30 minutes. Then **S11** (4-((6-bromohexyl)oxy)benzaldehyde, 4.20 mg, 17.1 μmol) and 10% TFA(trifluoroacetic acid) in $CH_2Cl_2$ (0.01 mL) were added. The mixture was further stirred at 25 °C for 48 h. Removal of solvents afforded an aurantia solid and the crude material was purified by trituration using petroleum ether. **[6]Rs** was obtained by filtration to as an aurantia solid. (28.0 mg, 91%). $^1$H NMR (400 MHz, $CDCl_3/CD_3CN$, 1:1, v/v, 298 K) δ 9.96 (s, 8H), 9.79 (s, 8H), 9.58 (s, 16H), 9.51(m, 8H),9.38 (m, 8H), 9.17 (s, 16H), 8.96 (s, 4H), 8.77 (s, 8H), 8.68 (s, 4H), 8.49 (s, 8H), 8.31 (s, 8H), 8.21 (s, 8H), 8.02 (s, 4H), 7.72 (s, 4H), 7.55 (s, 8H), 6.91 (m, 8H), 6.49 (s, 8H), 6.25 (s, 8H), 6.14 (s, 8H), 5.05 (s, 5H), 4.10 (m, 72H), 3.73 (m, 82H), 3.41 (t, 8H), 1.74 (m, 58H), 1.50 (m, 350H), 1.40 - 1.20 (m, 325H), 1.17 - 1.03 (m, 171H), 0.96 (m,82H), 0.86 (m, 75H). $^{13}$C NMR (100 MHz, $CDCl_3/CD_3CN$, 1:1, v/v, 298 K) δ 164.64, 159.76, 159.07, 158.86, 158.45, 158.30, 158.07, 157.75, 155.97, 154.86, 150.70, 144.98, 144.47, 144.09, 132.66, 128.76, 128.18, 125.86, 122.03, 120.81, 119.87, 119.32, 117.20, 115.25, 114.25, 113.72, 111.40, 71.82, 39.54, 39.45, 39.29, 38.49, 34.66, 33.02, 30.78, 30.74, 30.69, 30.28, 30.09, 29.23, 28.90, 28.70, 25.18, 24.69, 23.64, 23.53, 22.98, 22.93, 21.07, 13.89, 13.59, 11.29, 10.97, 10.78. ESI-HRMS: m/z calculated for $C_{582}H_{816}N_{76}O_{72}^{4+}$ $[M-4PF_6^-]^{4+}$ 2513.0631; found 2513.0767.

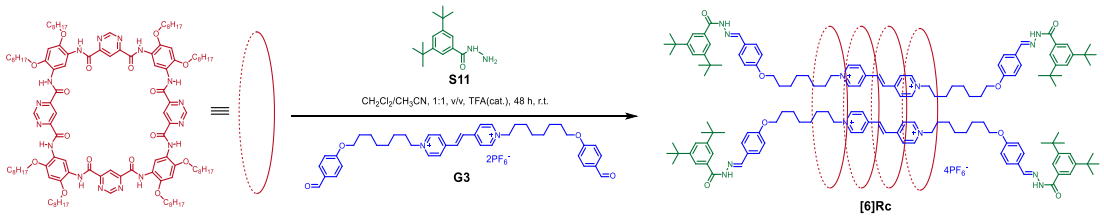


**Scheme S5** Synthetic route of doubly threaded [6]rotaxane **[6]Rc**.

**[6]Rs:** A mixture of macrocycle **1a** (24.8 mg, 12.5 μmol) and guest **G3** (5.30 mg, 5.70 μmol) and was stirred in dry $CH_2Cl_2/CH_3CN$ (1:1, v/v, 18 mL) at room temperature for 30 minutes. Then **S11** (4-((6-bromohexyl)oxy)benzaldehyde, 4.20 mg, 17.1 μmol) and 10% TFA(trifluoroacetic acid) in $CH_2Cl_2$ (0.01 mL) were added. The mixture was further stirred at 25 ˚C for 48 h. Removal of solvents afforded an aurantia solid and the crude material was purified by trituration using petroleum ether. **[6]Rs** was obtained by filtration to as an aurantia solid. (27.2 mg, 89 %).$^1$H NMR (400 MHz, $CDCl_3/CD_3CN$, 1:1, v/v, 298 K) δ 9.93 (s, 8H), 9.78 (s, 8H), 9.58 (s, 16H), 9.51 (s, 8H), 9.33 (s, 8H), 9.19 (s, 16H), 8.95 (s, 4H), 8.77 (s, 16H), 8.51 (s, 8H), 8.35 (s, 8H), 8.26 (s, 8H), 8.11 (s, 4H), 7.71 (s, 4H), 7.60 (d, J = 16.7 Hz, 16H), 7.23 (s, 8H), 6.92 (s, 2H), 6.53 (s, 8H), 6.28 (s, 16H), 5.02 (s, 4H), 4.13-3.89 (m, 31H), 3.77 (m, 75H), 3.33 (m, 8H), 1.75 (m, 53H), 1.51 (m, 308H), 1.45 - 1.18 (m, 371H), 1.20 - 1.03 (m, 185H), 0.95 (dd, J = 13.3, 6.6 Hz, 83H), 0.90 - 0.69 (m, 106H). $^{13}$C NMR (100 MHz, $CDCl_3/CD_3CN$, 1:1, v/v, 298 K) δ 165.33, 159.49, 158.95, 158.45, 158.30, 158.07, 157.75, 156.16, 155.77, 151.56, 150.78, 145.73, 144.87, 144.47, 143.69, 132.66, 129.33, 128.18, 126.55, 125.86, 121.57, 121.43, 119.94, 119.32, 116.13, 115.58, 114.68, 113.72, 112.04, 97.04, 95.17, 72.21, 68.47, 67.02, 39.54, 39.45, 39.29, 34.66, 34.55, 31.25, 30.69, 30.58, 30.28, 30.09, 29.22, 28.90, 28.73, 28.70, 23.64, 23.53, 22.98, 22.93, 22.10, 14.96, 13.59, 11.89, 10.97, 10.78. ESI-HRMS: m/z calculated for $C_{592}H_{832}N7_6O_{72}^{4+}$ $[M\text{-}4PF_6^-]^{4+}$ 2541.3465; found 2541.1227.

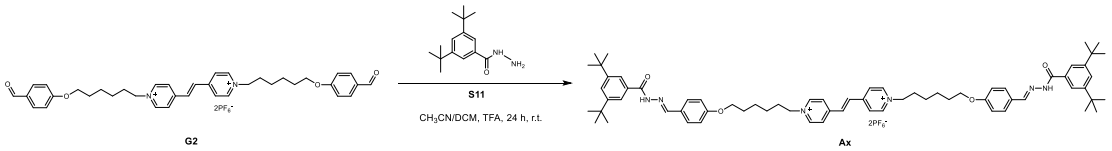


**Scheme S6** Synthetic route of the axle **Ax** of **[6]Rs**.

**Ax:** A mixture of **G2** (30 mg, 0.034 mmol), 4-((6-bromohexyl)oxy)benzaldehyde **S11** (17 mg, 0.068 mmol) in 10 mL $CH_3CN$/DCM (2:1, v/v) was added 10% TFA in $CH_2Cl_2$(1 mL) and stirred at room temperature for 24 h. The solvent was evaporated under reduced pressure to afford **Ax** as a light brown soild (nearly quantification) $^1$H NMR (400 MHz, $CDCl_3/CD_3CN$, 1:1, v/v, 298 K) δ 8.69 (d, *J* = 5.2 Hz, 4H), 8.28 (s, 1H), 8.18 (d, *J* = 5.2 Hz, 4H), 7.81 (s, 2H), 7.72 (d, *J* = 1.8 Hz, 4H), 7.67 (d, *J* = 9.0 Hz, 7H), 6.90 (d, *J* = 9.0 Hz, 4H), 4.51 (t, *J* = 7.3 Hz, 4H), 3.99 (t, *J* = 6.2 Hz, 4H), 2.02 (t, *J* = 7.4 Hz, 4H), 1.78 (p, *J* = 6.5 Hz, 4H), 1.57 – 1.48 (m, 4H), 1.43 (q, *J* = 9.0, 8.5 Hz, 4H), 1.37 (s, 36H). $^1$H NMR (100 MHz, $CDCl_3/CD_3CN$, 1:1, v/v, 298 K) δ161.40, 158.96, 150.71, 150.17, 148.87, 127.10, 125.93, 121.13, 116.81, 114.51, 68.97, 61.29, 37.11, 33.71, 30.79, 30.70, 30.28, 28.27, 25.70, 24.96. ESI-HRMS: m/z calculated for $C_{68}H_{88}N_6O_4^{2+}$ $[M\text{-}2PF_6^-]^{2+}$ 526.3482; found 526.3411.

# 3. Spectroscopic Characterization

## 3.1 $^{1}H$ and $^{13}C$ NMR Spectra

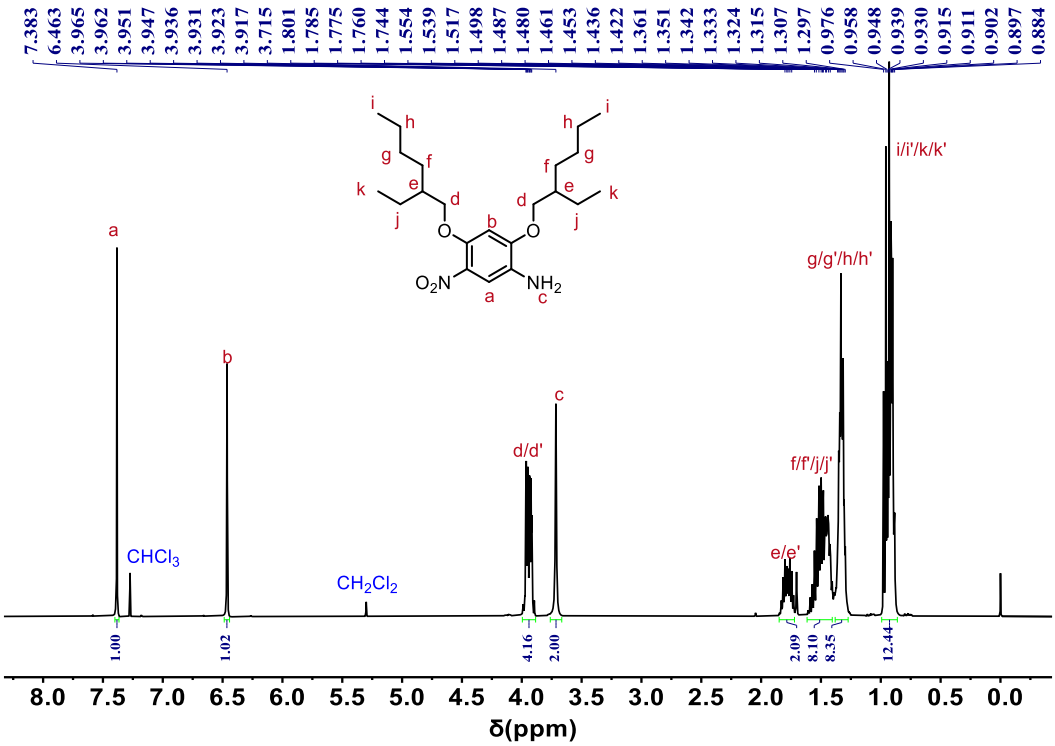


**Figure S1** $^{1}H$ NMR spectrum of **S2** (400 MHz, $CDCl_3$, 298K).

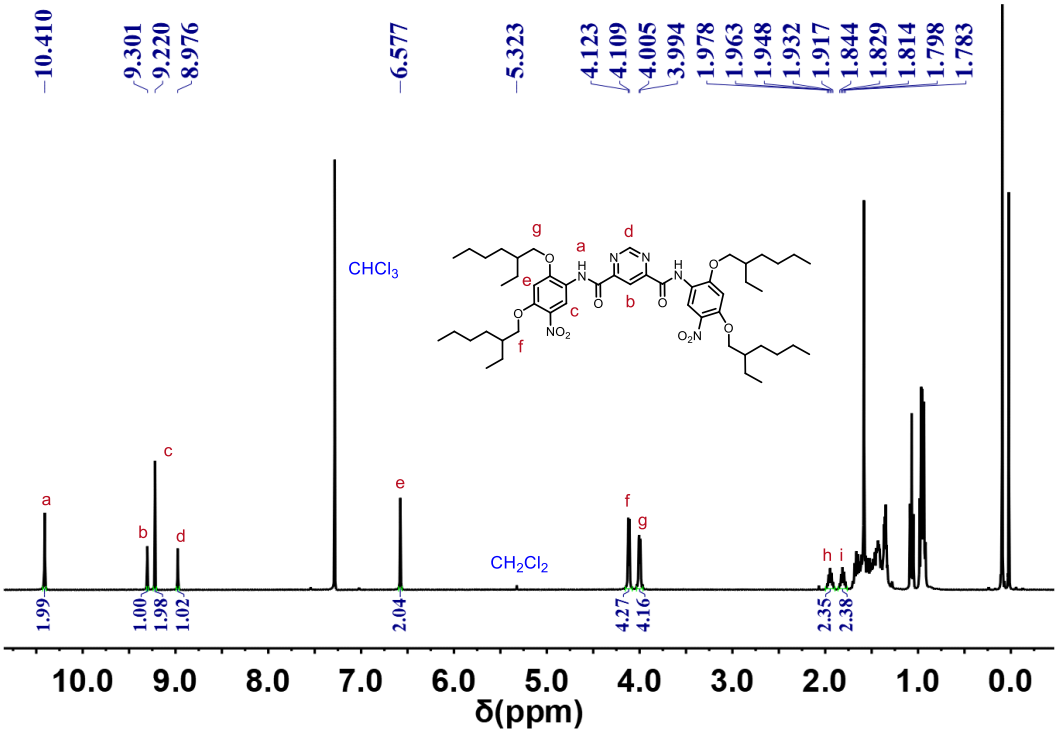


**Figure S2** $^{1}H$ NMR spectrum of **S5** (400 MHz, $CDCl_3$, 298K).

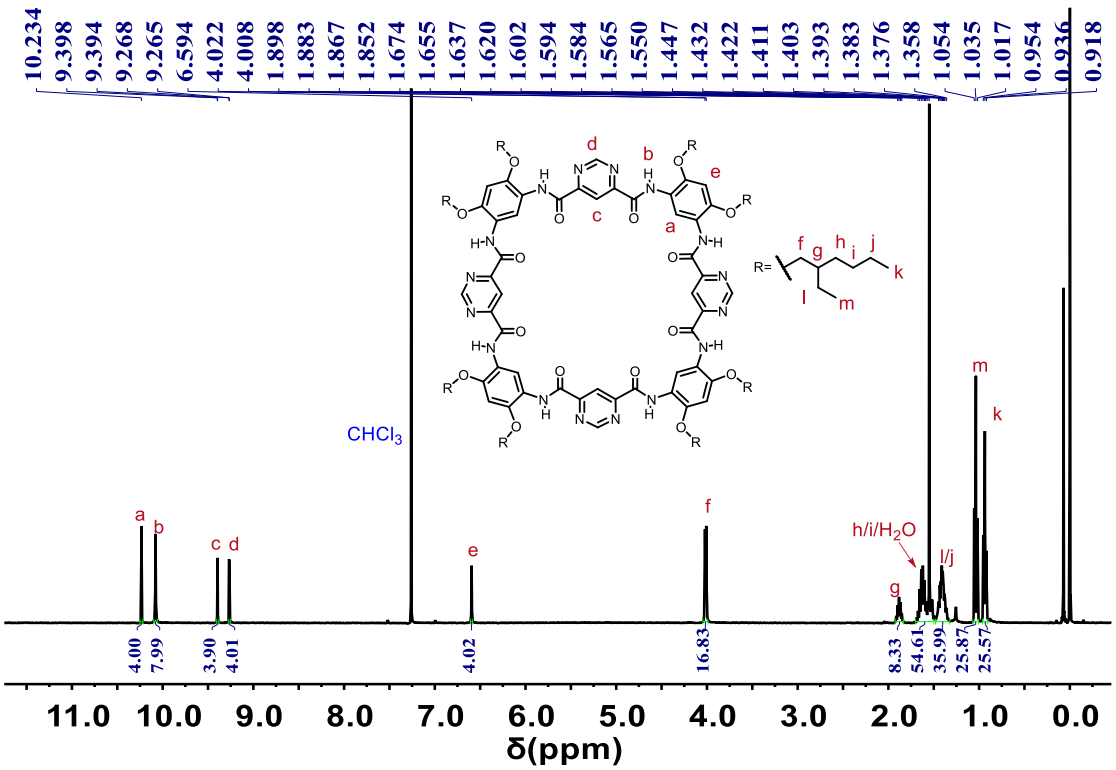


**Figure S3** $^{1}$H NMR spectrum of **1a** (400 MHz, $CDCl_3$, 298K).

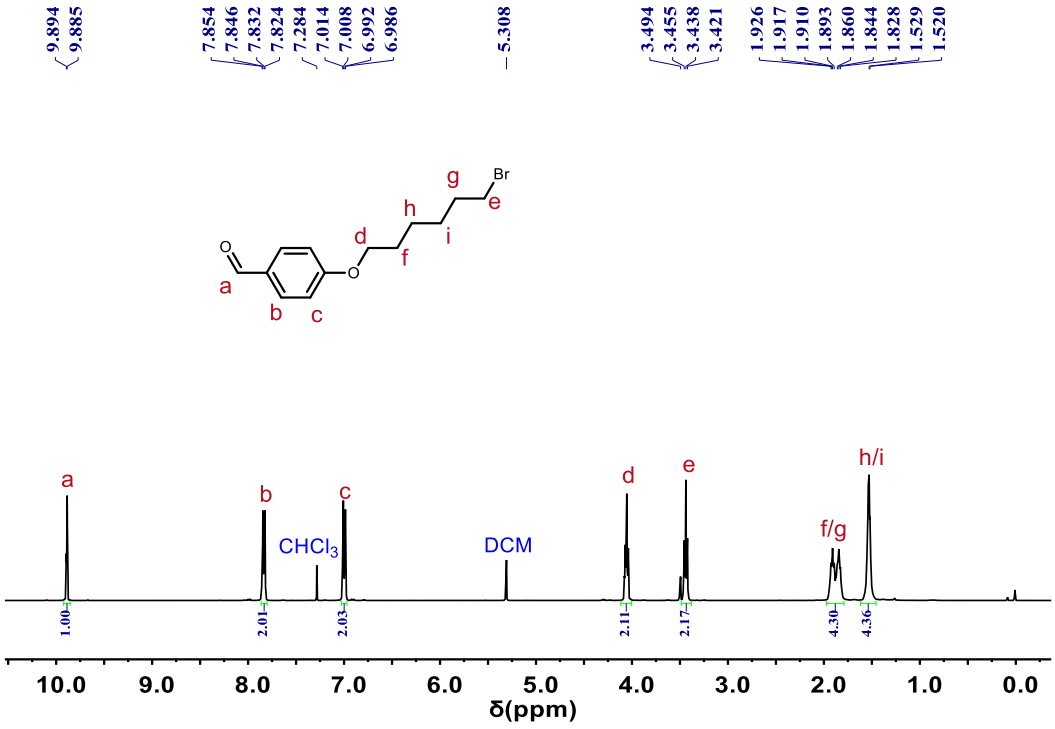


**Figure S4** $^{1}$H NMR spectrum of **S9** (400 MHz, $CDCl_3$, 298K).

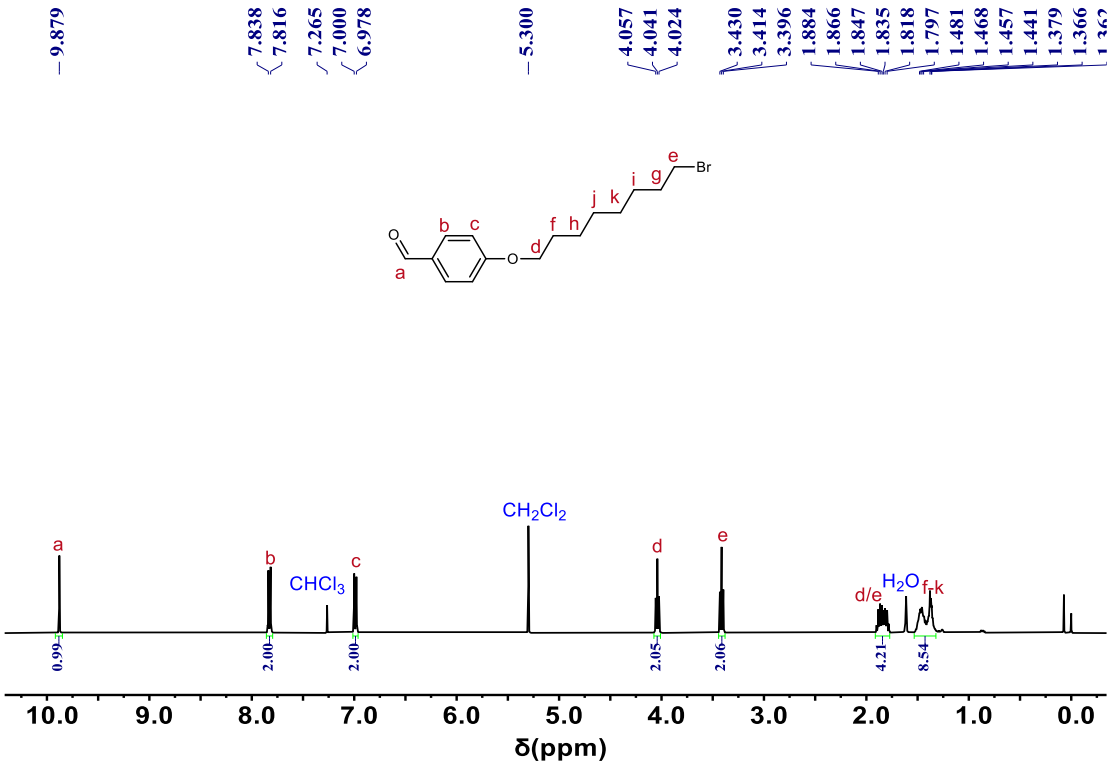


**Figure S5** [1]H NMR spectrum of **S10** (400 MHz, $CDCl_3$, 298K).

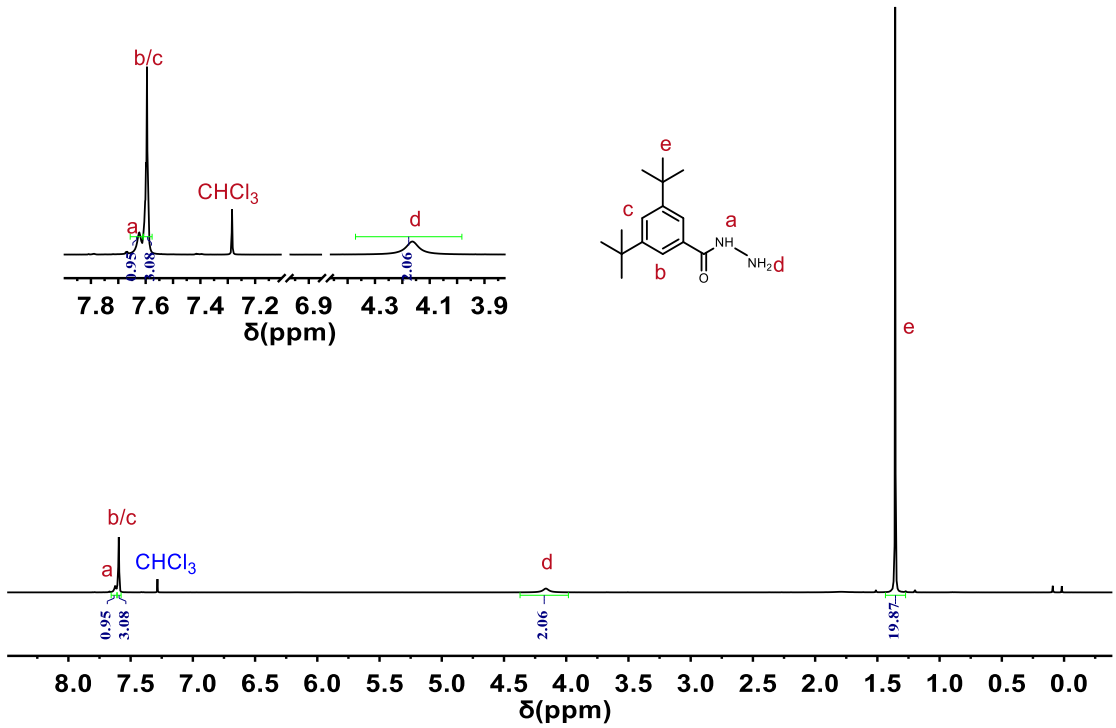


**Figure S6** [1]H NMR spectrum of **S11** (400 MHz, $CDCl_3$, 298K).

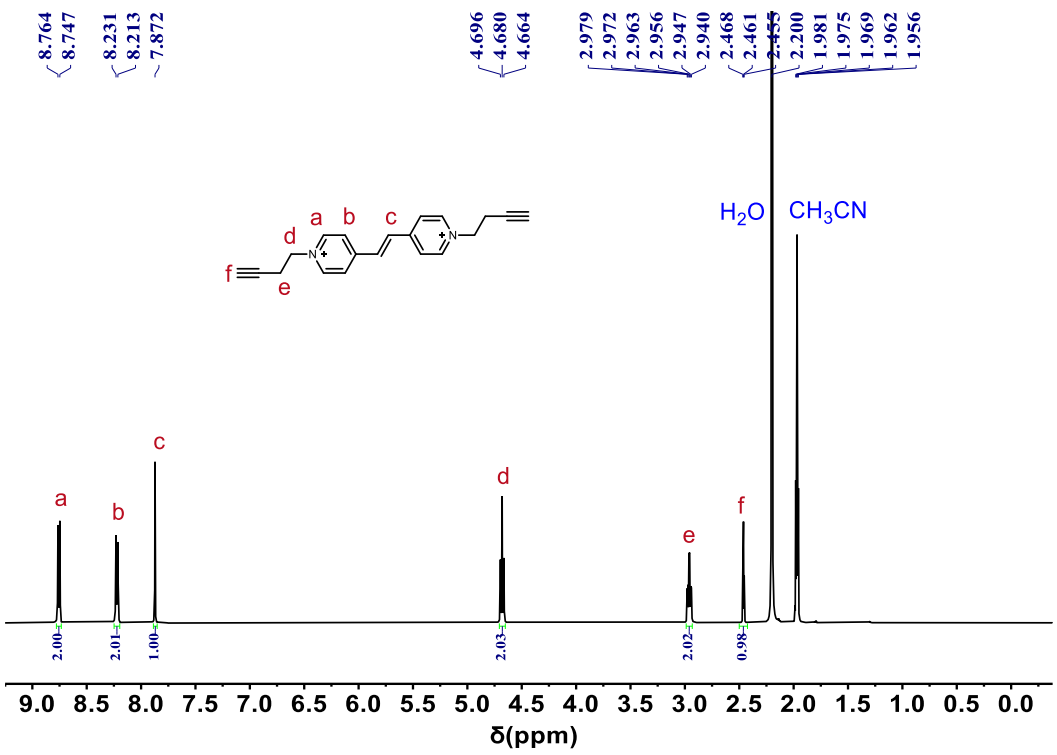


**Figure S7** $^{1}$H NMR spectrum of **G1** (400 MHz, $CD_3CN$, 298K).

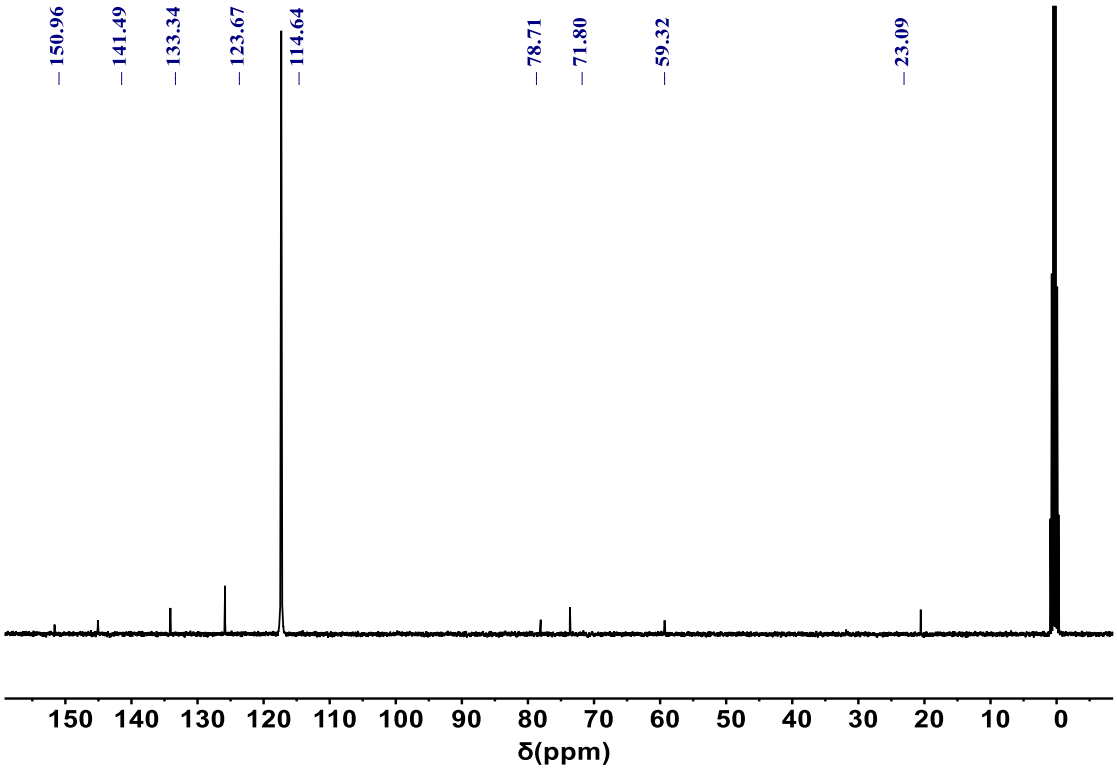


**Figure S8** $^{13}$C NMR spectrum of **G1** (100 MHz, $CD_3CN$, 298 K).

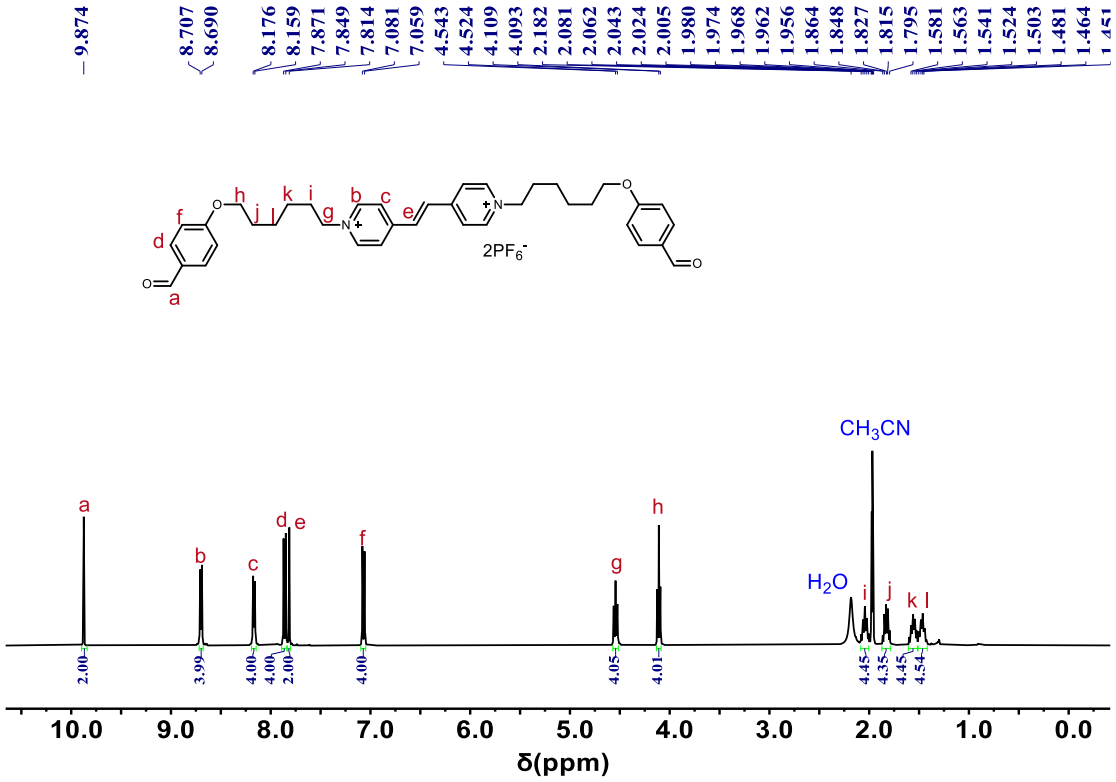


**Figure S9** $^{1}$H NMR spectrum of **G2** (400 MHz, $CD_3CN$, 298K).

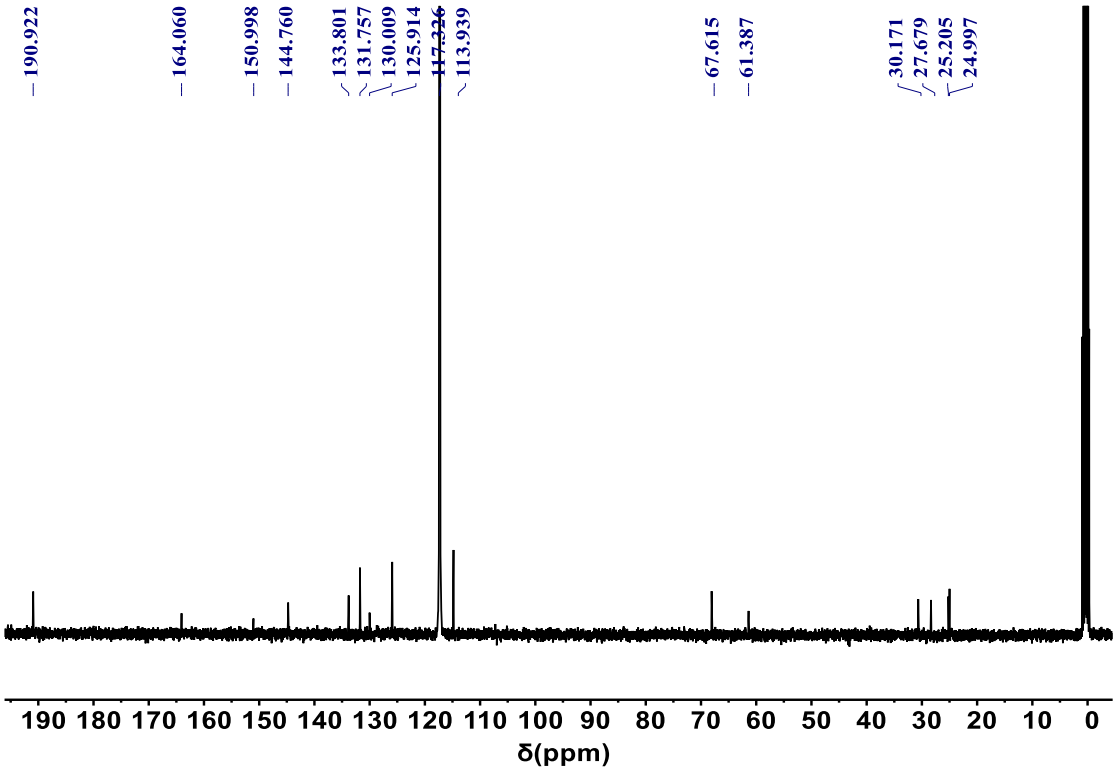


**Figure S10**$^{13}$C NMR spectrum of **G2** (100 MHz, $CD_3CN$, 298 K).

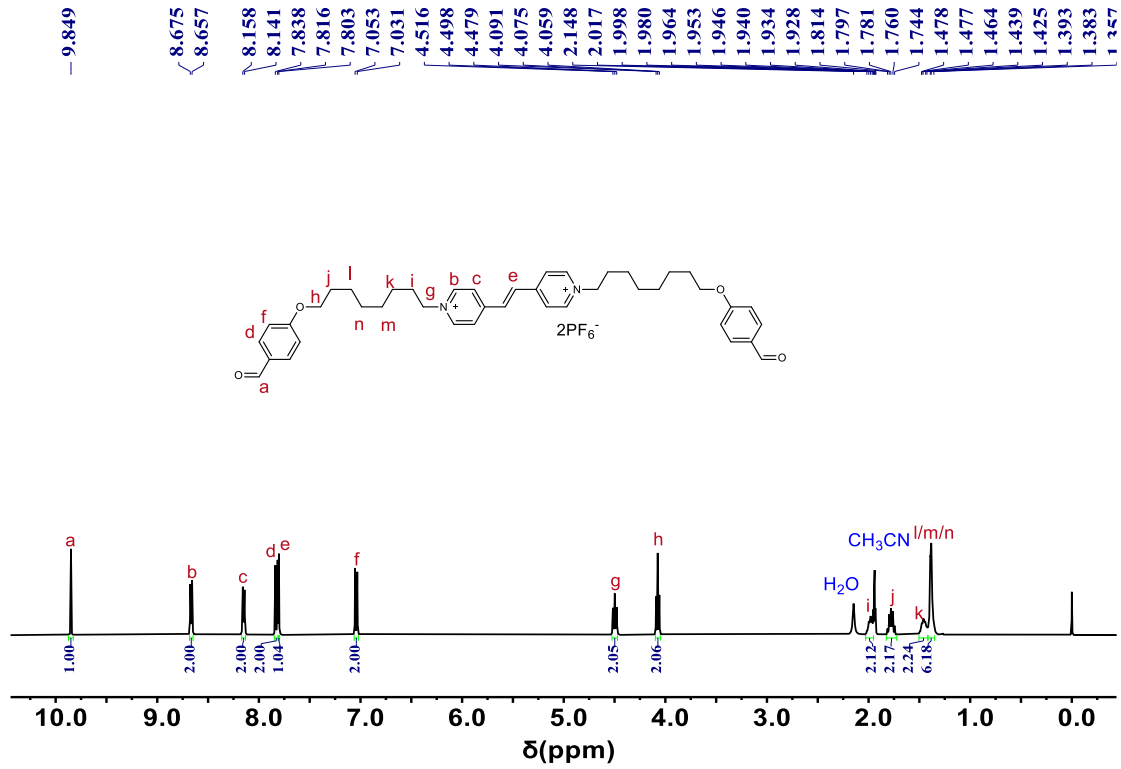


**Figure S11**[1]H NMR spectrum of **G3** (400 MHz, $CD_3CN$, 298K).

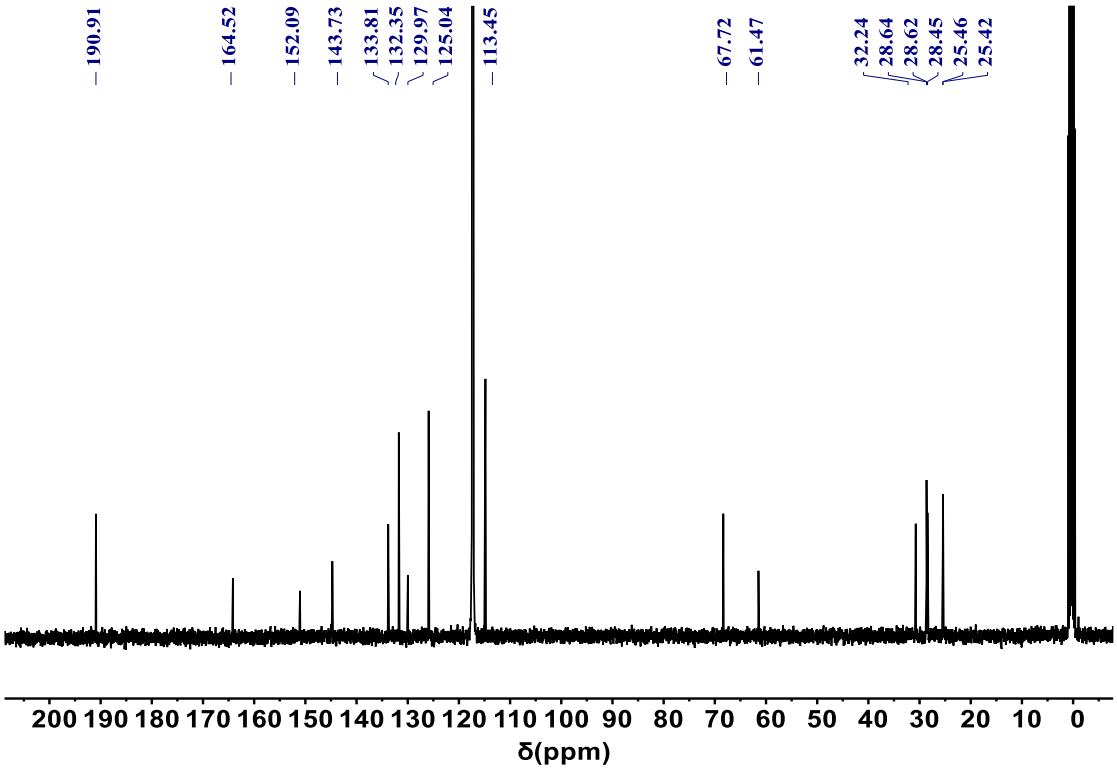


**Figure S12**[13]C NMR spectrum of **G3** (100 MHz, $CD_3CN$, 298 K).

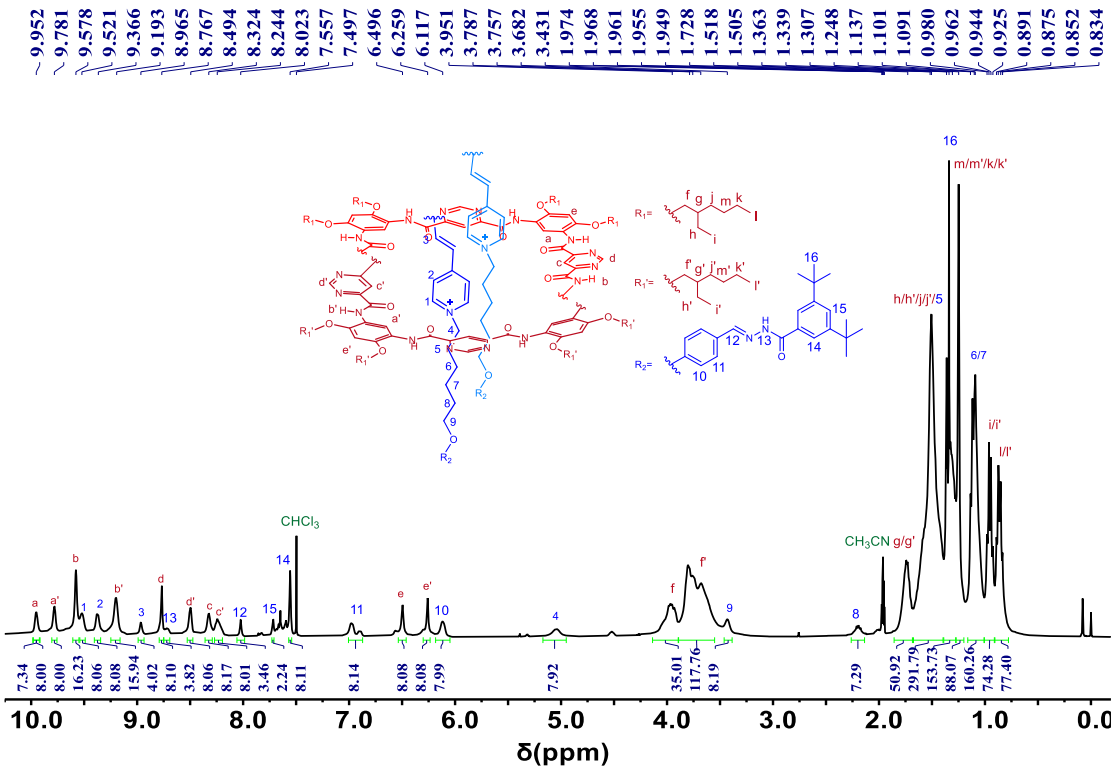


**Figure S13** $^{1}$H NMR spectrum of **[6]Rs** (400 MHz, $CDCl_3/CD_3CN$, 1:1, v/v, 298K).

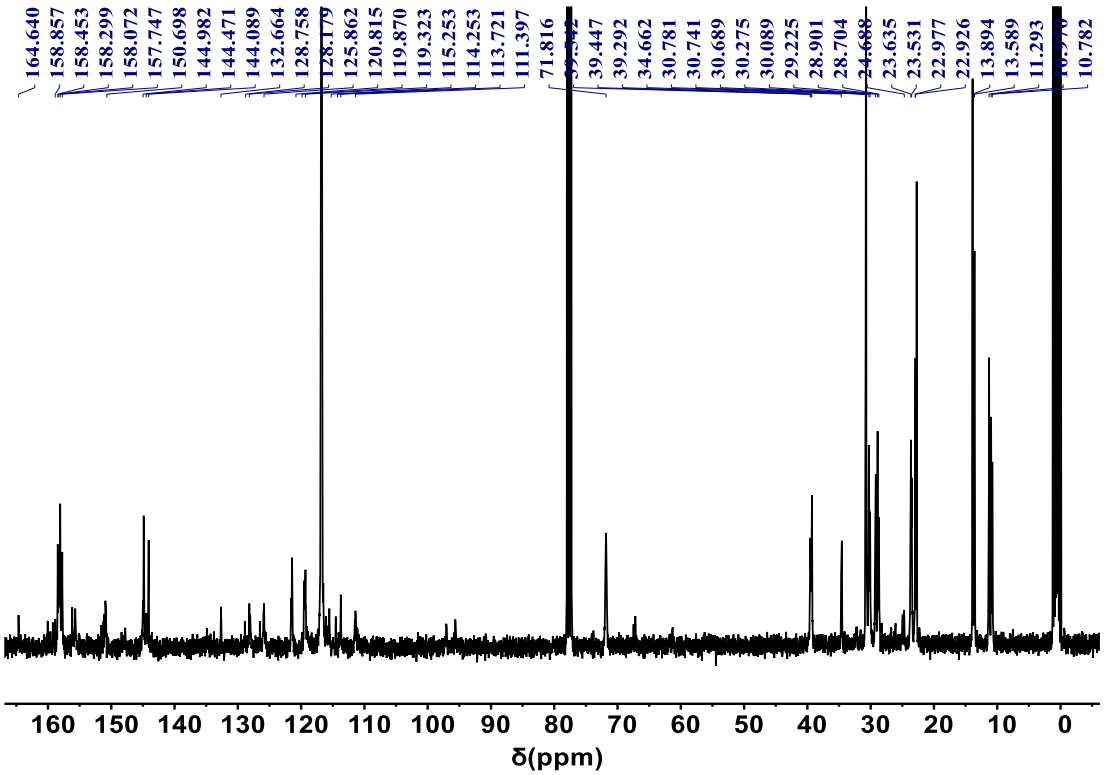


**Figure S14** $^{13}$C NMR spectrum of **[6]Rs** (100 MHz, $CDCl_3/CD_3CN$, 1:1, v/v, 298 K).

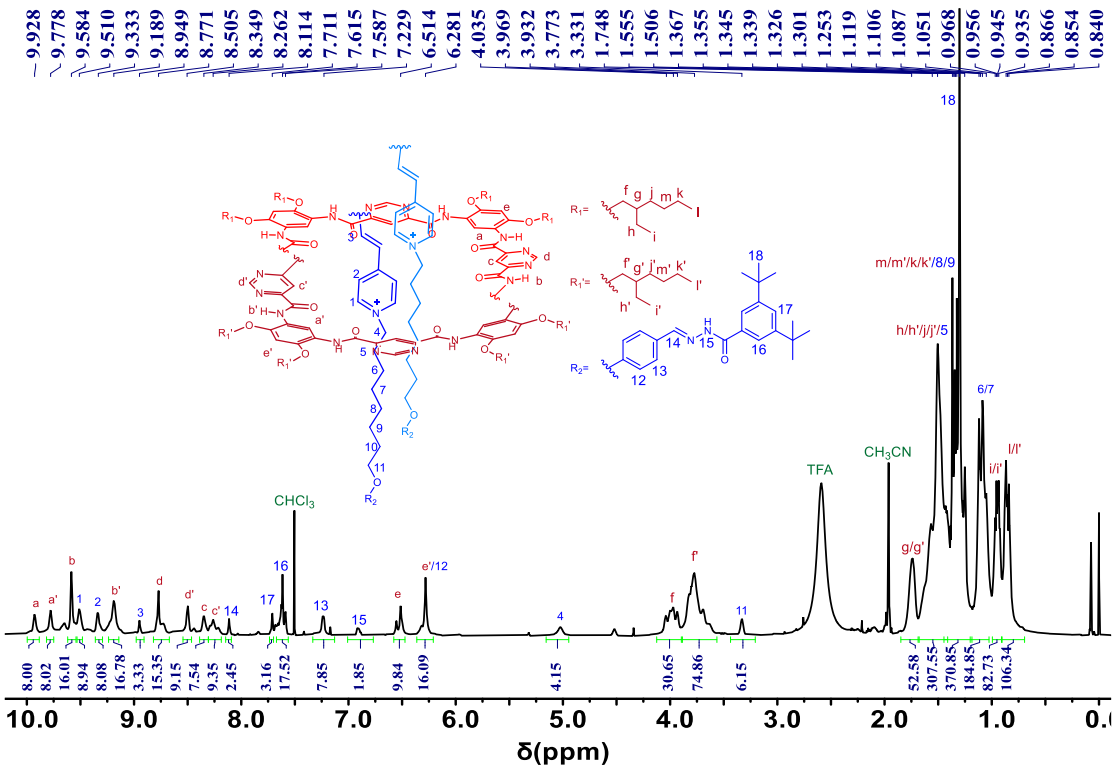


**Figure S15** $^{1}$H NMR spectrum of **[6]Rc** (400 MHz, $CDCl_3/CD_3CN$, 1:1, v/v, 298K).

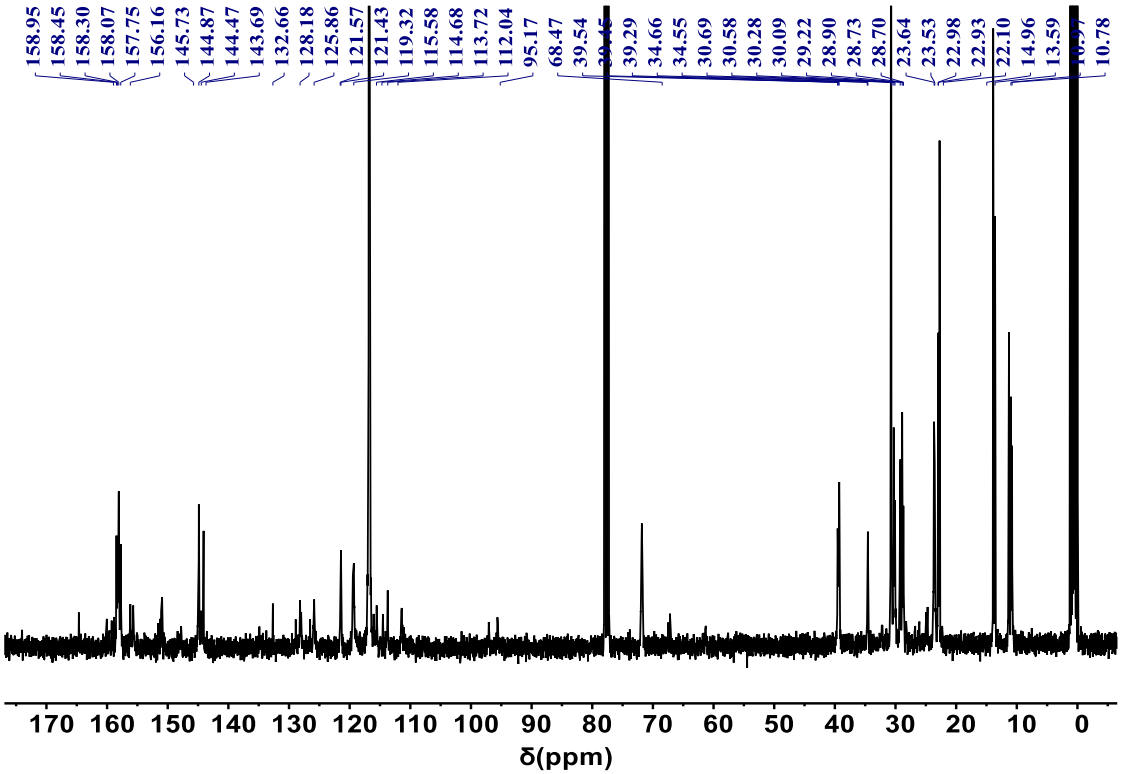


**Figure S16** $^{13}$C NMR spectrum of **[6]Rc** (100 MHz, $CDCl_3/CD_3CN$, 1:1, v/v, 298 K).

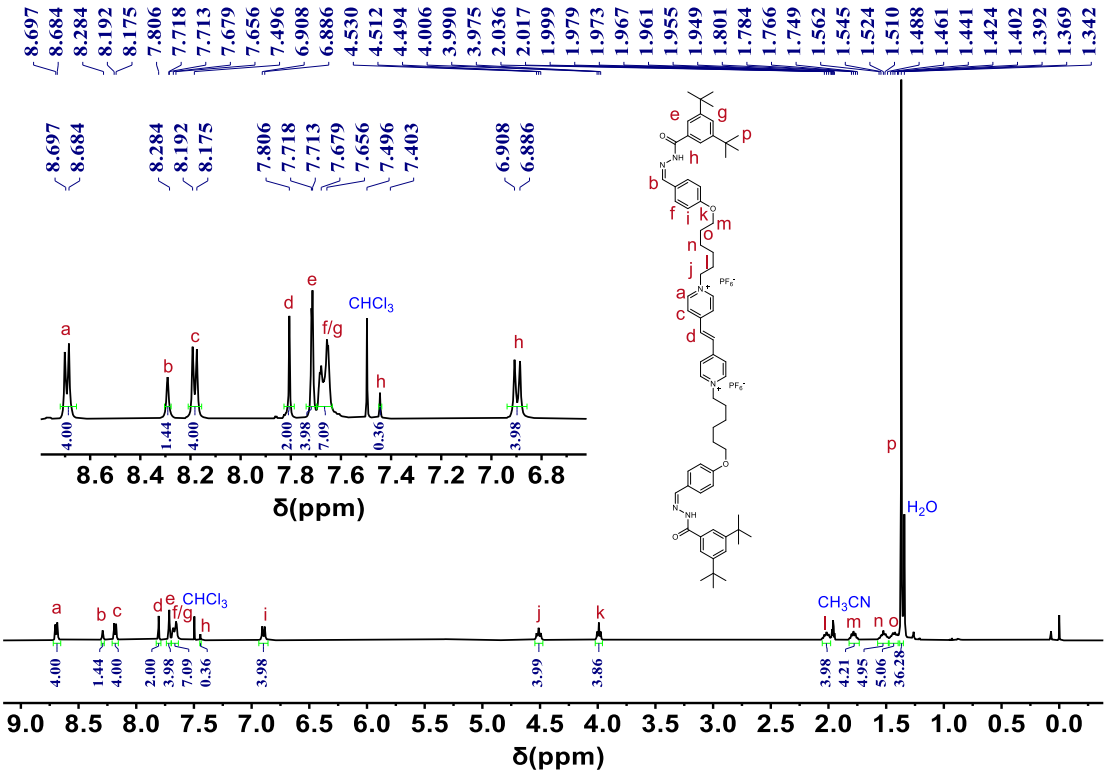


**Figure S17** $^{1}$H NMR spectrum of **Ax** (400 MHz, $CDCl_3/CD_3CN$, 1:1, v/v, 298K).

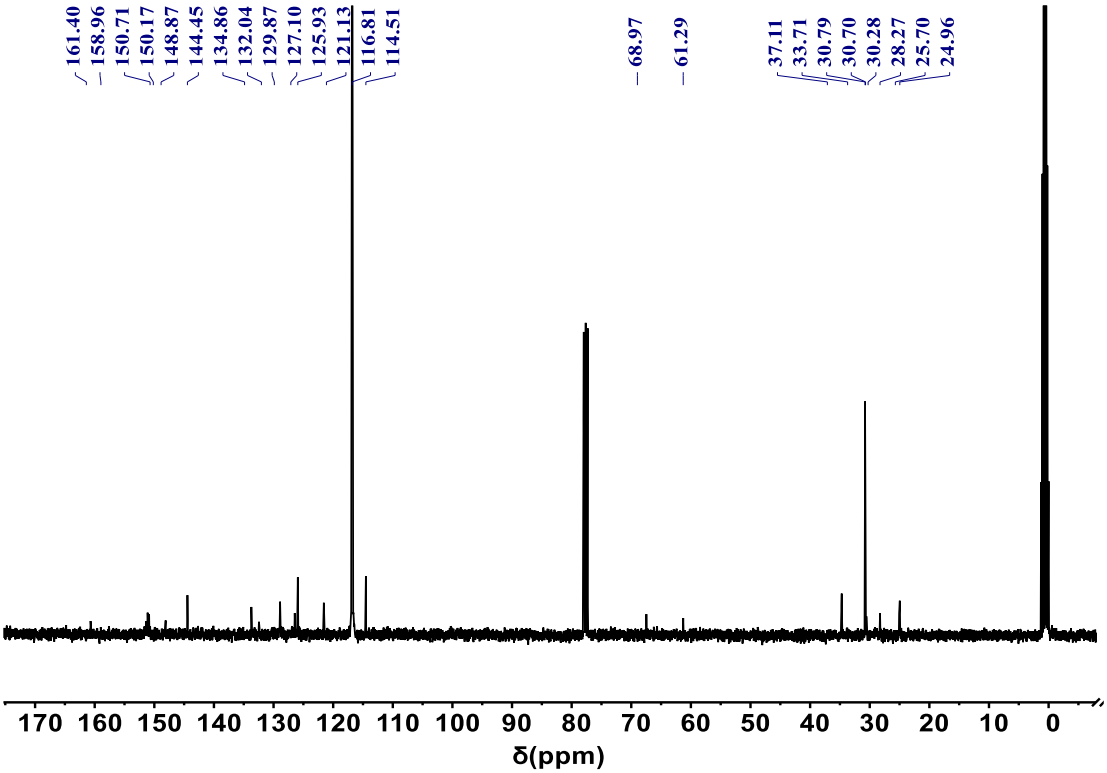


**Figure S18** $^{13}$C NMR spectrum of **Ax** (400 MHz, $CDCl_3/CD_3CN$, 1:1, v/v, 298K).

## 3.2 ESI-HRMS Spectra

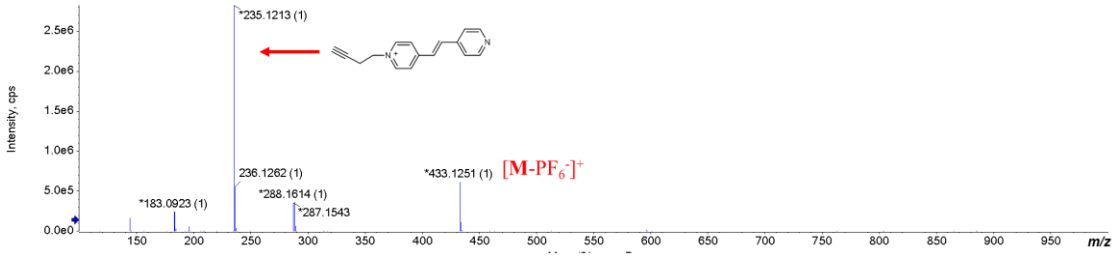


**Figure S19** ESI-HRMS spectrum of **G1**.

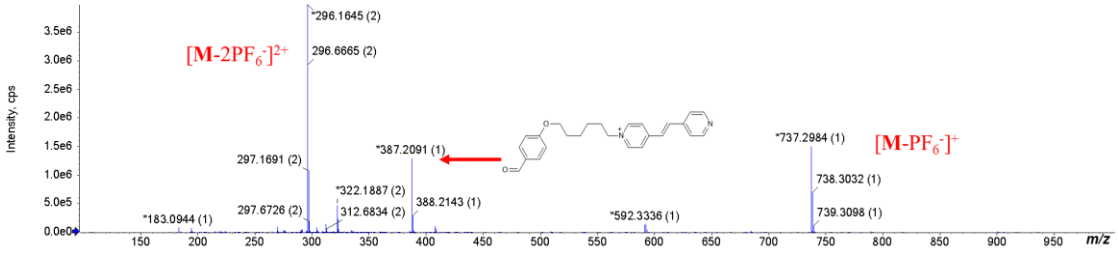


**Figure S20** ESI-HRMS spectrum of **G2**.

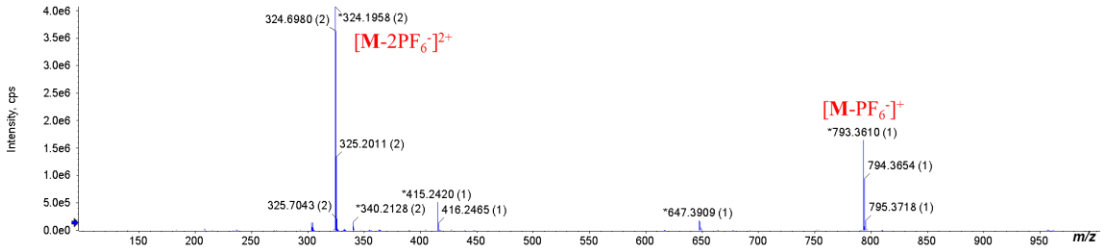


**Figure S21** ESI-HRMS spectrum of **G3**.

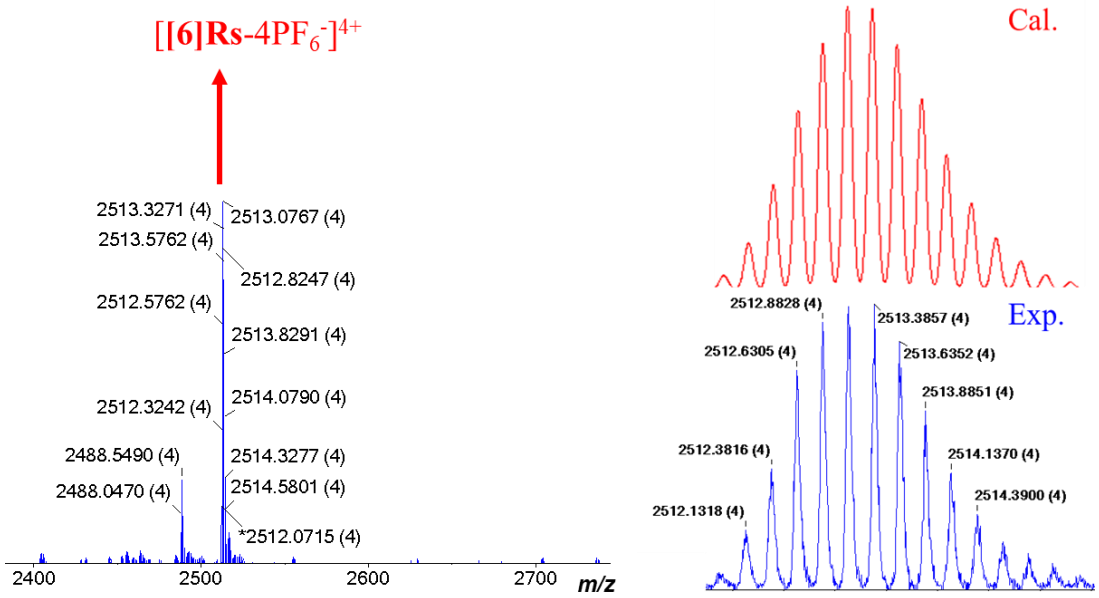


**Figure S22** ESI-HRMS spectrum of **[6]Rs**.

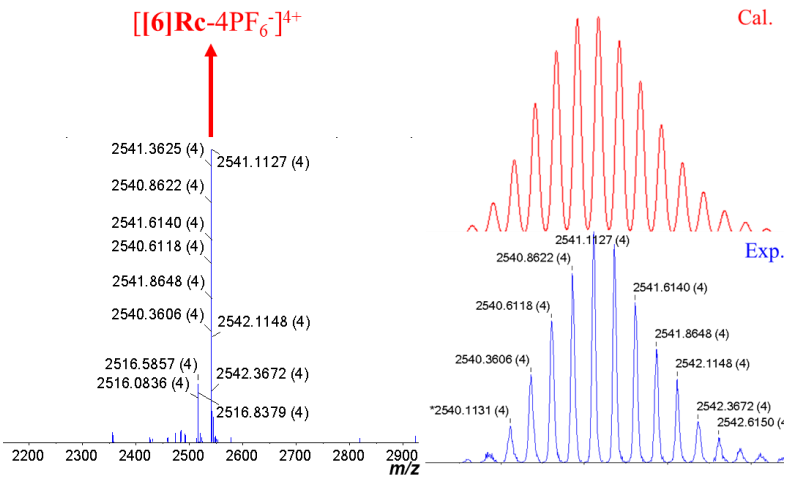


**Figure S23**ESI-HRMS spectrum of **[6]Rc**.

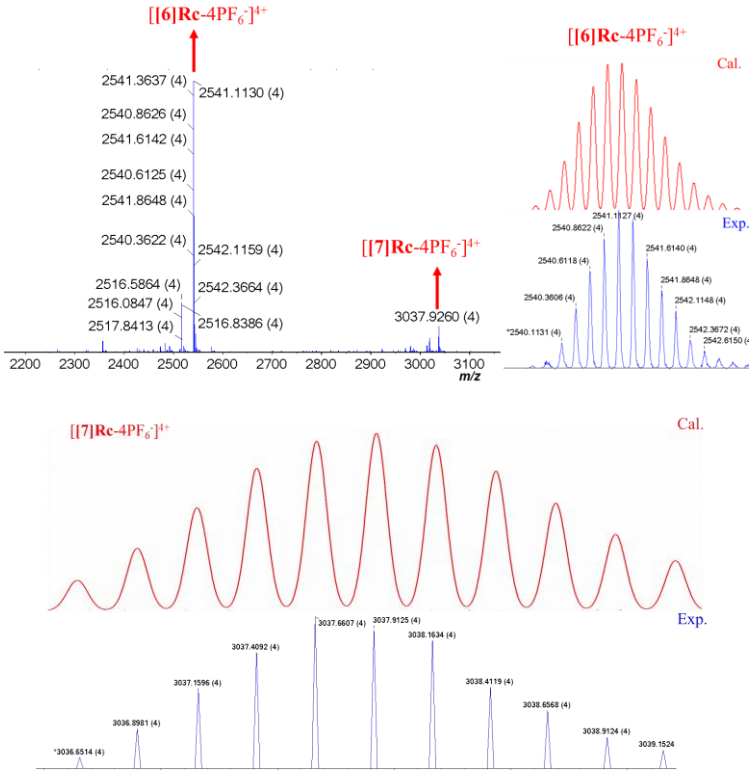


**Figure S24** ESI-HRMS spectrum of the mixture of **[6]Rc** and **[7]Rc**.

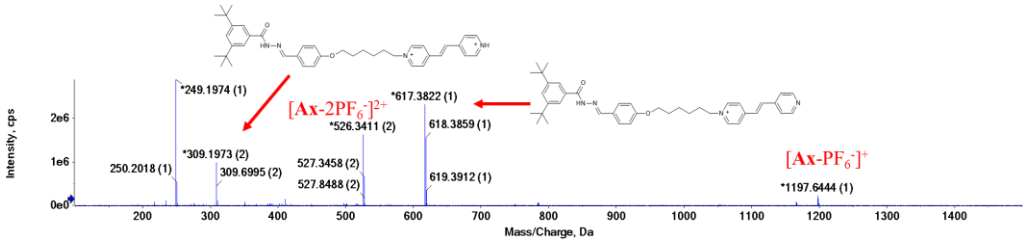


**Figure S25** ESI-HRMS spectrum of **Ax**.

# 4. Host-Guest Complexation of 1a and G1-G3

## 4.1 Color Change of Complexes

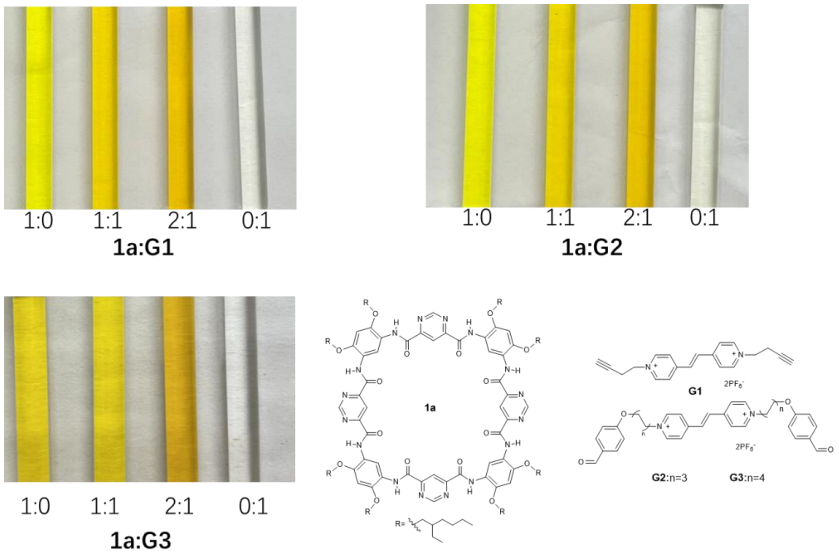


**Figure S26** Color change of the complexes formed from **1a** and **G1**-**G3**.

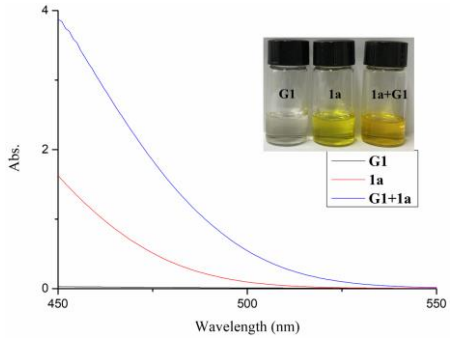


**Figure S27** The UV-vis spectrum of **G1** (0.1 mM, black line), **1a** (0.2 mM, red line), **1a** + **G1** (0.1 mM for **G1** and 0.2 mM for **1a**, blue line) in ($CDCl_3$/$CD_3CN$, 1:1, v/v) at 298 K.

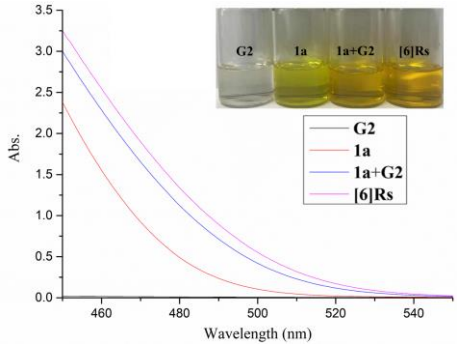


**Figure S28** The UV-vis spectrum of **G2** (0.1 mM, black line), **1a** (0.2 mM, red line), **1a** + **G2** (0.1 mM for **G2** and 0.2 mM for **1a**, blue line), **[6]Rs** (0.05 mM, pink line) in ($CDCl_3$/$CD_3CN$, 1:1, v/v) at 298 K.

The molar extinction coefficients at 495 nm($\varepsilon_{495}$) of **1a**, **G1**, **G1**+**1a**, **G2**, **G2**+**1a** and **6[R]s** are calculated using Lamberbier's law and are shown in Table S1.

**Table S1** Molar extinction coefficients at 495 nm ($\varepsilon_{495}$) of **1a**, **G1**, **G1**+**1a**, **G2**, **G2**+**1a** and **6[R]s**

| | $Abs._{495}$ | $\varepsilon_{495}$ ( $L\ mol^{-1}\ cm^{-1}$) |
|---|---|---|
| **1a** | 0.139 | 695 |
| **G1** | 0.013 | 130 |
| **G1**+**1a** | 0.625 | 12500 |
| **G2** | 0.008 | 80 |
| **G2**+**1a** | 0.553 | 11060 |
| **6[R]s** | 0.710 | 14200 |

### 4.2 NMR Spectra of Complexes

Since the solubility of **1a** alone in $CDCl_3/CD_3CN$ (1:1, v/v) is too low to allow acquisition of the $^1H$ NMR signals, titration experiments were performed in nine individual NMR tubes by adding indicated aliquots of the stock solution of **1a** in $CHCl_3$ (0.5 mM) by means of a Hamilton syringe to 100 μL solution of the guest (**G1**-**G3**) in $CH_3CN$. The solutions were mixed well by ultrasonication. Then all the mixed solvents were removed under vacuum and 500 μL of $CDCl_3/CD_3CN$ (1:1, v/v) was added to each NMR tube. After homogenization and equilibration, $^1H$ NMR spectra were recorded at 298 K. The stock solutions of **1a** and guests **G1**-**G3** were freshly prepared and the concentrations were 0.5 mM.

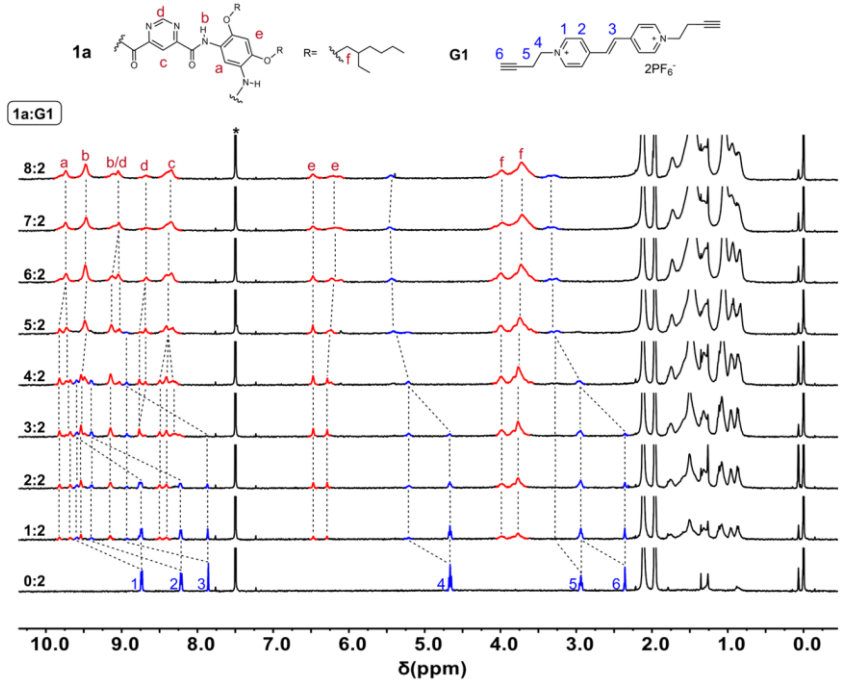


**Figure S29** Stacked $^1H$ NMR spectra ($CDCl_3/CD_3CN$, 1:1, v/v, 400 MHz, 298 K) of **G1** titrated with **1a**. ([**G1**] = 5 × $10^{-4}$ M, [**1a**]/[**G1**] = 0 - 4). The spectrum of **1a** alone was not acquired due to limited solubility. Asterisk denotes the solvent peak.

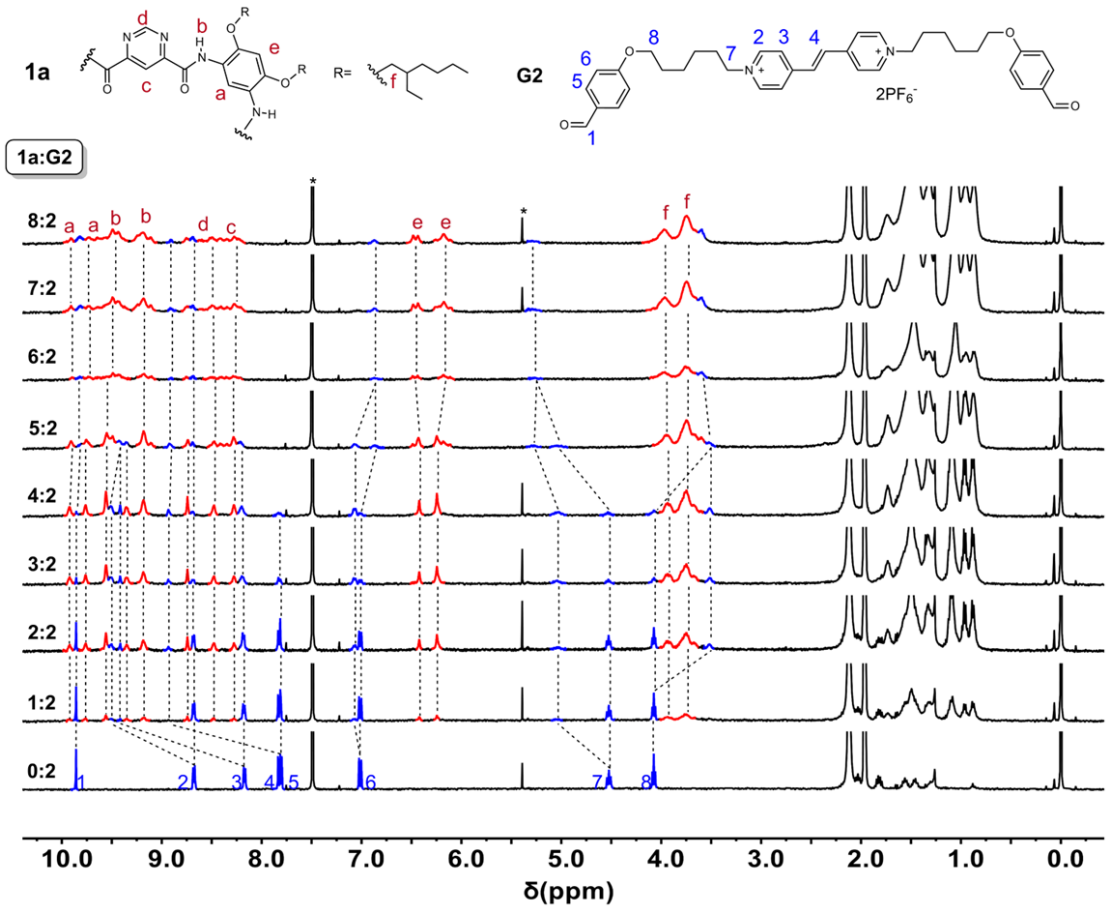


**Figure S30** Stacked $^{1}$H NMR spectra ($CDCl_3/CD_3CN$, 1:1, v/v, 400 MHz, 298 K) of **G2** titrated with **1a**. ([**G2**] = 5 × $10^{-4}$ M, [**1a**]/[**G2**] = 0 - 4). The spectrum of **1a** alone was not acquired due to limited solubility. Asterisk denotes the solvent peak.

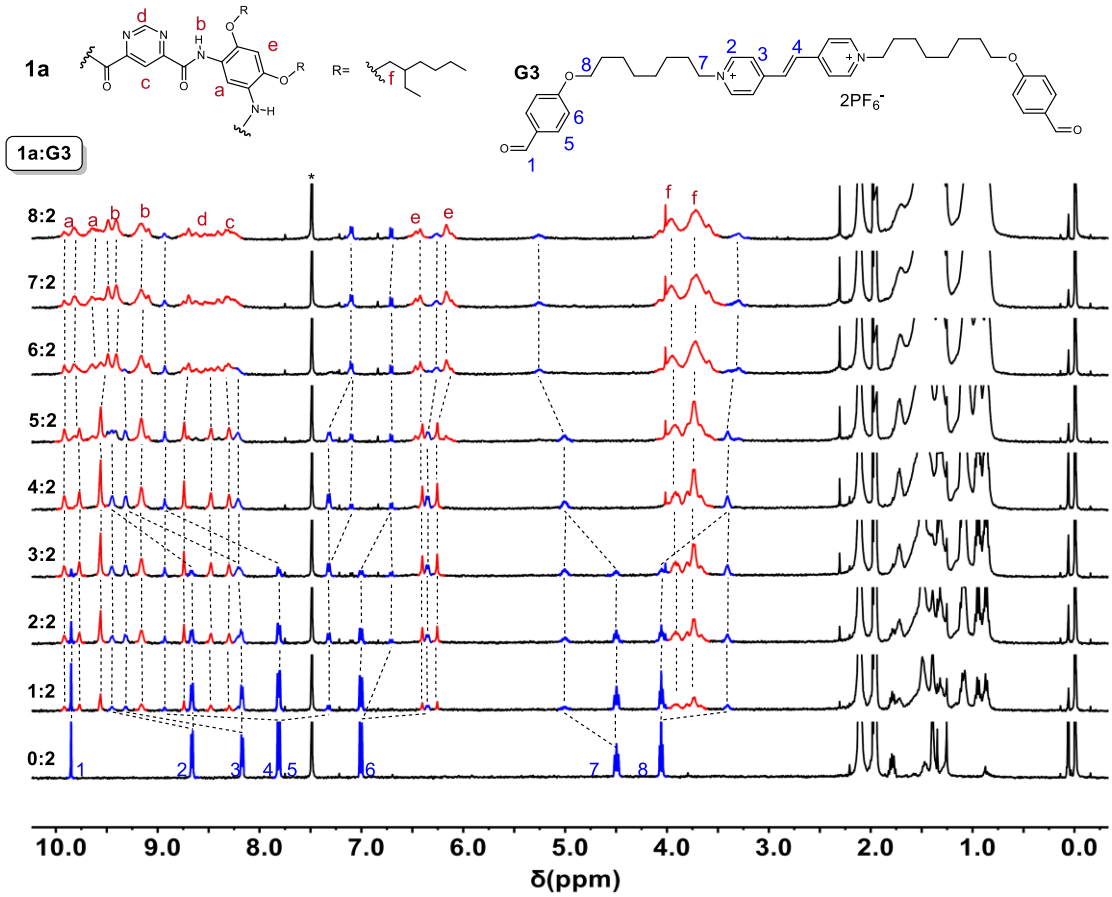


**Figure S31** Stacked $^{1}$H NMR spectra ($CDCl_3/CD_3CN$, 1:1, v/v, 400 MHz, 298 K) of **G3** titrated with **1a**. ([**G3**] = 5 × $10^{-4}$ M, [**1a**]/[**G3**] = 0 - 4). The spectrum of **1a** alone was not acquired due to limited solubility. Asterisk denotes the solvent peak.

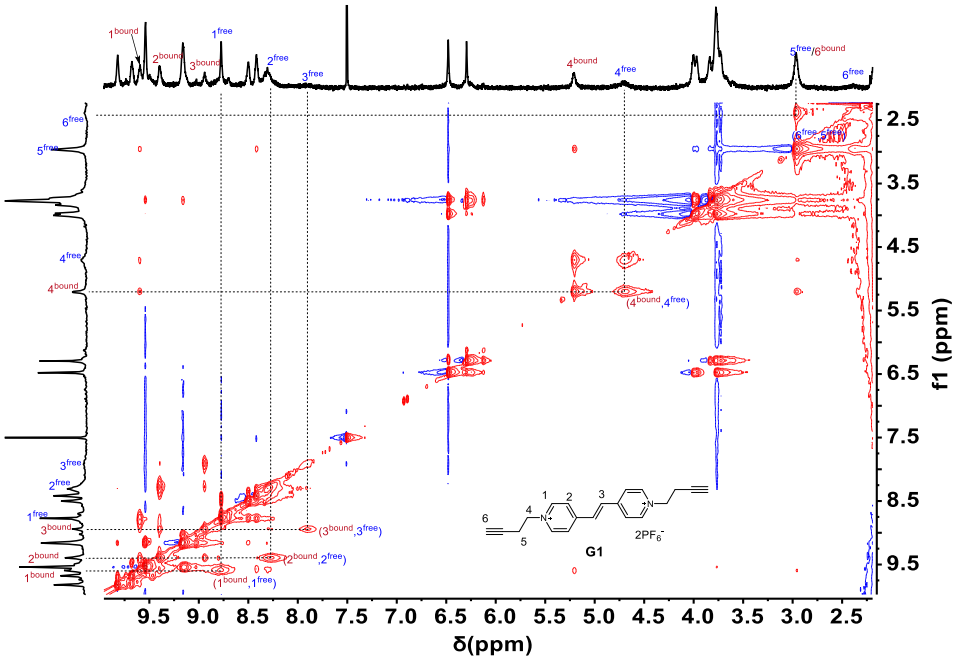


**Figure S32** Expanded 2D ROESY spectrum of **1a** and **G1**(**1a** : **G1**=3 : 2, 600 MHz, $CDCl_3/CD_3CN$,1 : 1, v/v, 298 K, 10 mM, mixing time = 0.4 s).

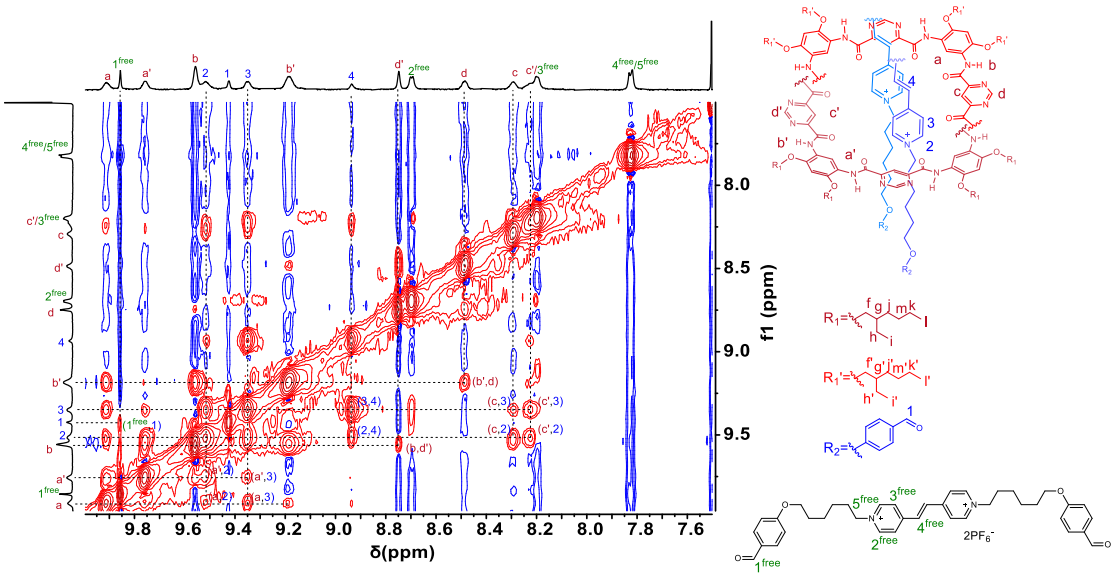


**Figure S33** Expanded 2D ROESY spectrum of **1a** and **G2**(**1a** : **G2**=3 : 2, 600 MHz, $CDCl_3/CD_3CN$,1 : 1, v/v, 298 K, 10 mM, mixing time = 0.4 s)

## 4.3 ESI-HRMS Spectra of Complexes

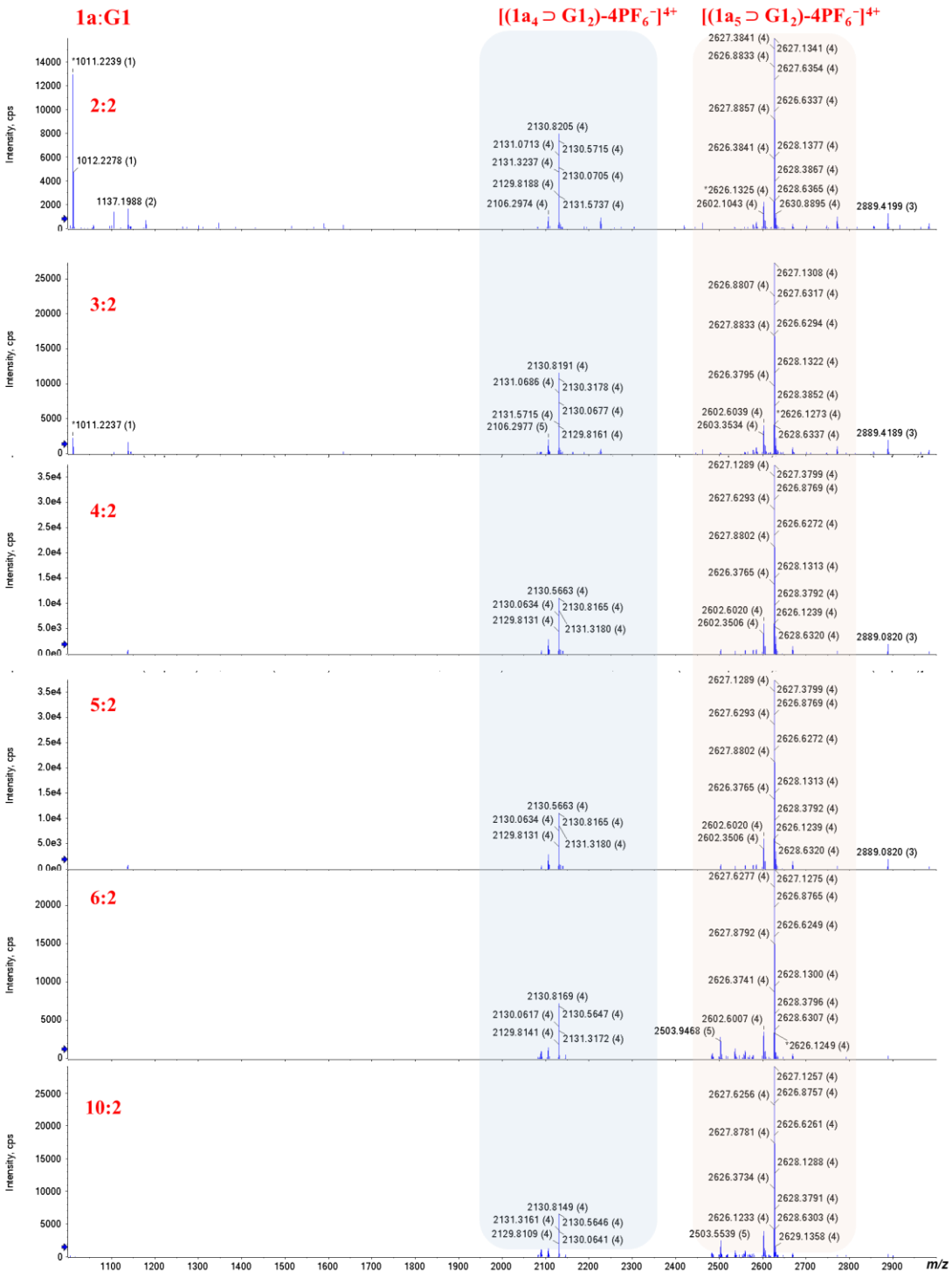


**Figure S34** ESI-HRMS spectra of **1a** and **G1** at different equivalents

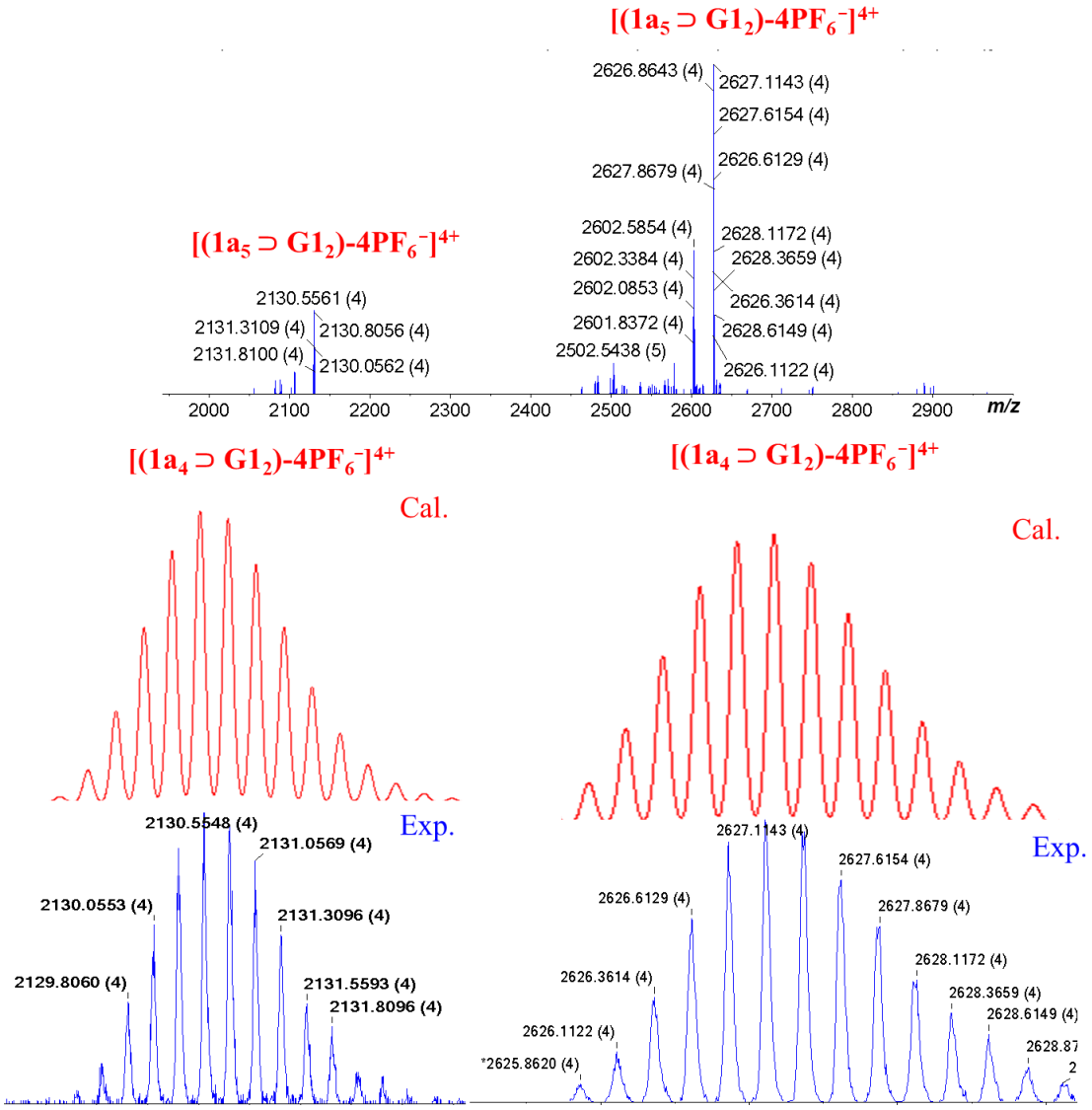


**Figure S35** ESI-HRMS spectrum of complexes **1a$_4$ ⊃ G1$_2$** and **1a$_5$ ⊃ G1$_2$**.

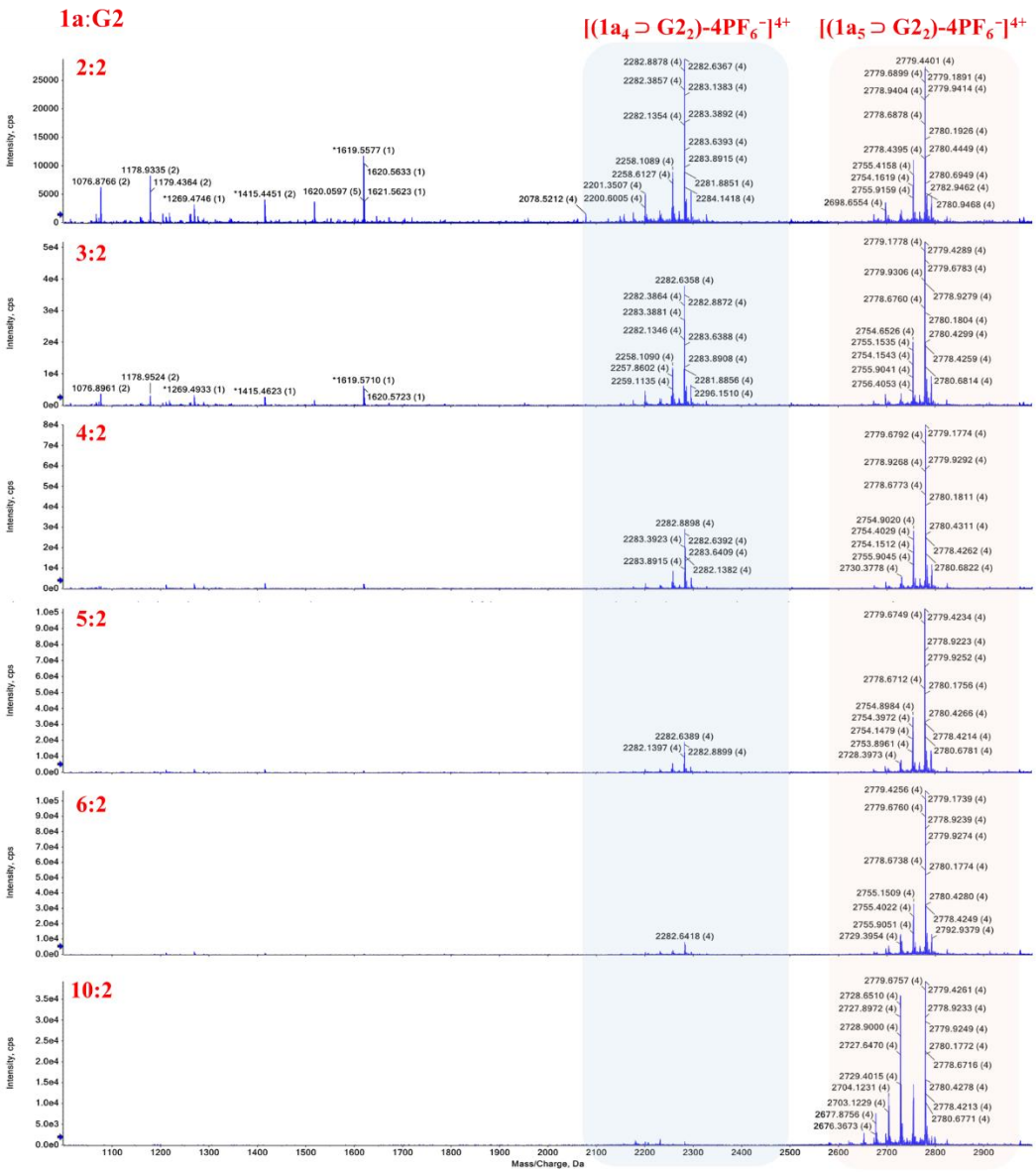


**Figure S36** ESI-HRMS spectra of **1a** and **G2** at different equivalents.

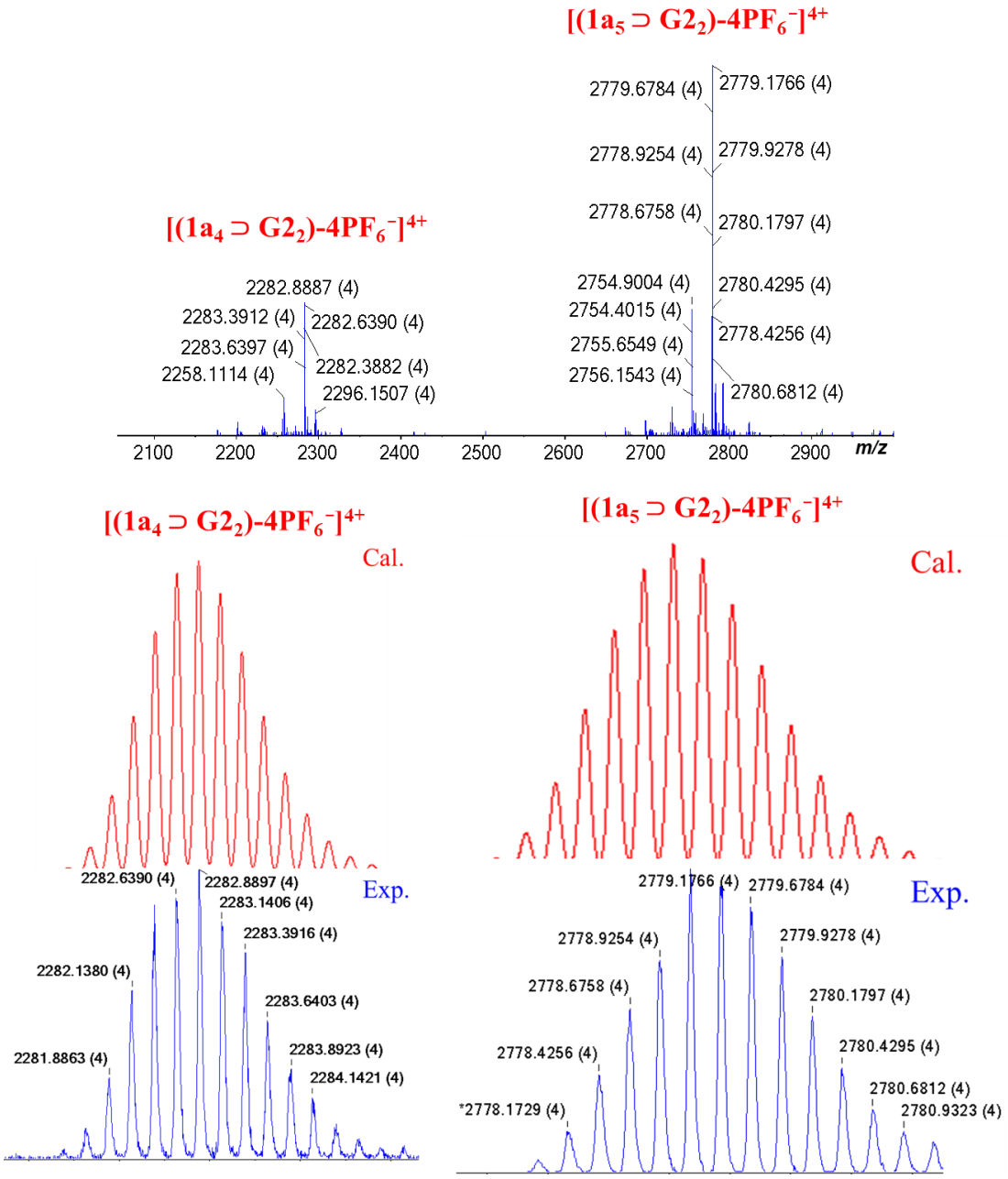


**Figure S37** ESI-HRMS spectra of complexes **1a**$_4$ ⊃ **G2**$_2$ and **1a**$_5$ ⊃ **G2**$_2$.

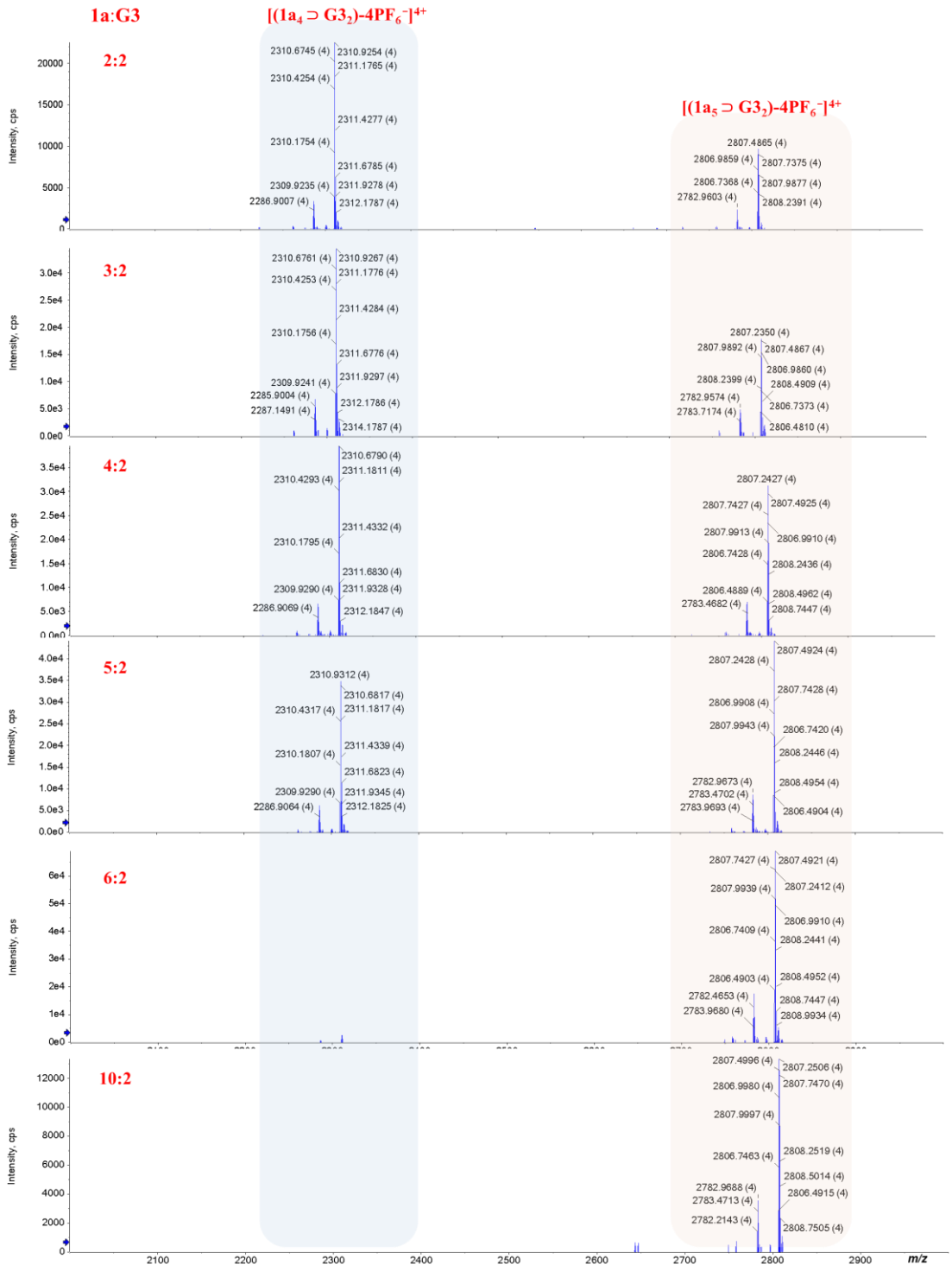


**Figure S38** ESI-HRMS spectra of **1a** and **G3** at different equivalents.

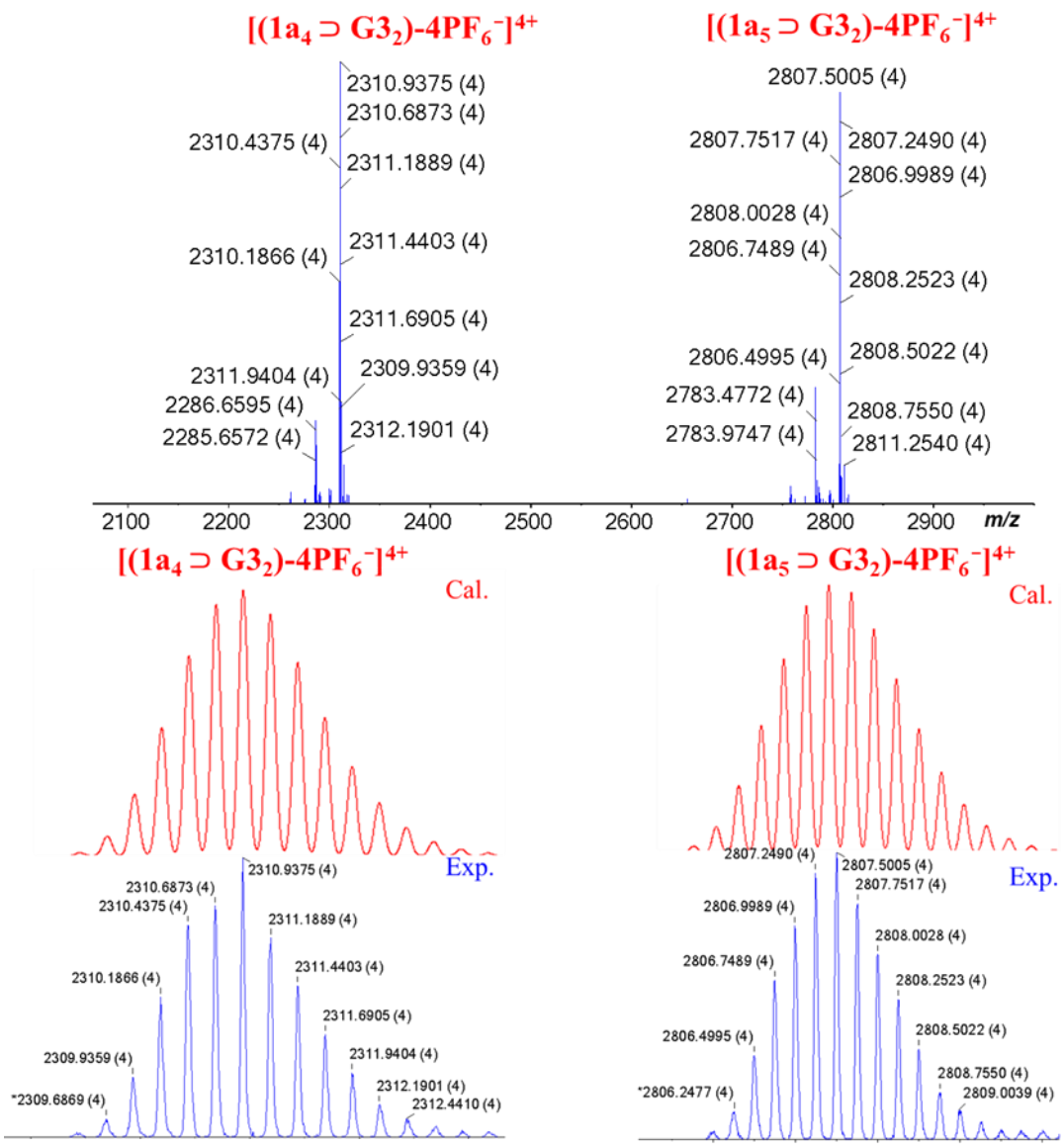


**Figure S39** ESI-HRMS spectra of complexes **1a4 ⊃ G32** and **1a5 ⊃ G32**.

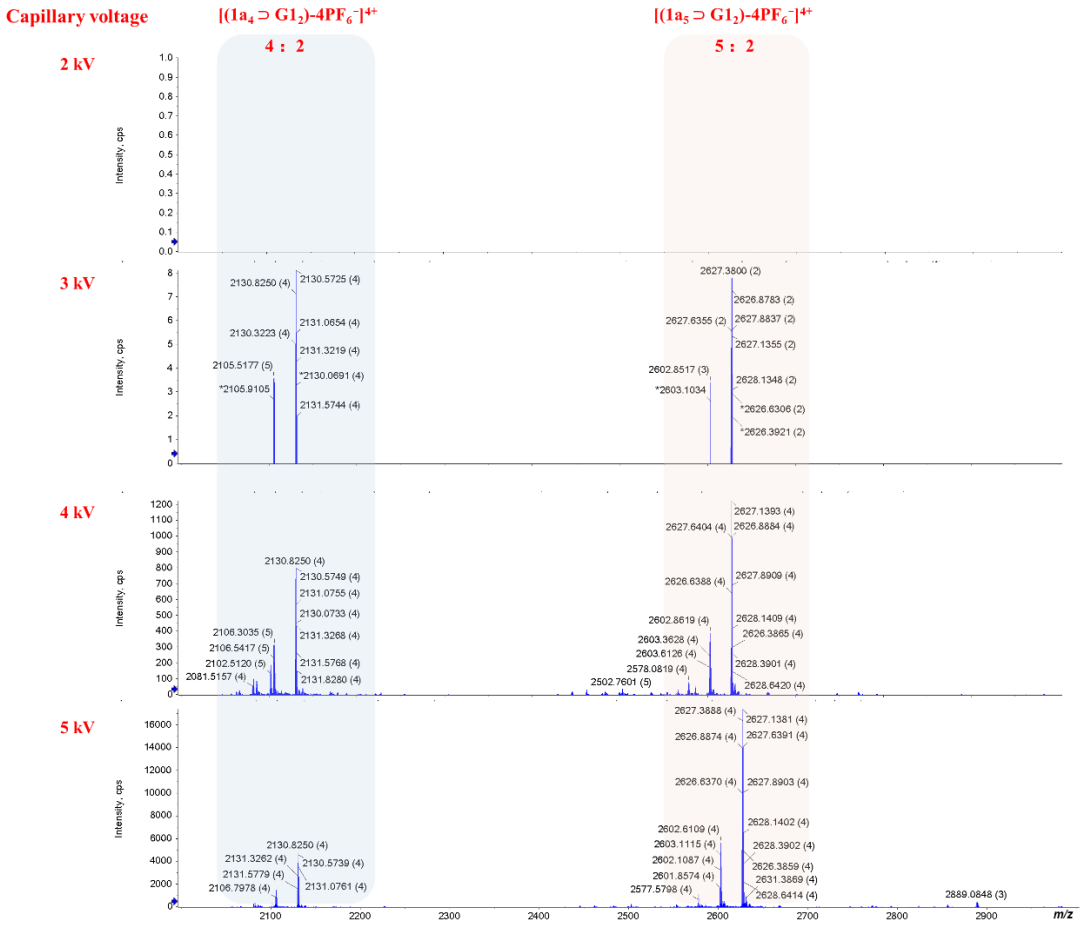


**Figure S40** ESI-HRMS of **1a** and **G1** at the molar ratio of 2:1 at different capillary voltage.

## 4.4 Job Plots of Host-Guest Complexes

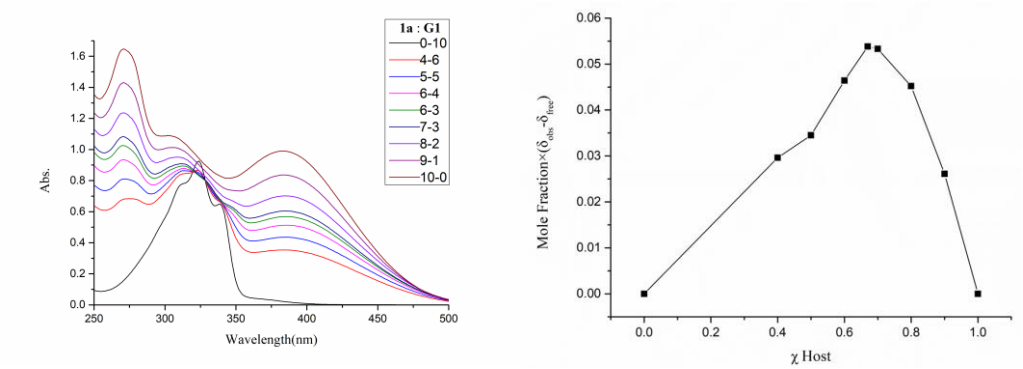


**Figure S41** Job plot analysis of the stoichiometric ratio between **1a** and **G1** in a solution of $CHCl_3/CH_3CN$ (1:1, v/v) at 298 K. The total concentration of **1a** and **G1** is held constant ([**1a**] + [**G1**] = 2.5 × $10^{-5}$ M. Absorbance intensity changes of **1a** recorded at 330 nm was used to analyze the binding ratio. The maximum on the Job plot lies at molar fraction around 0.67~0.71, pointing to the presence of both 4 : 2 and 5 : 2 H-G complexes.

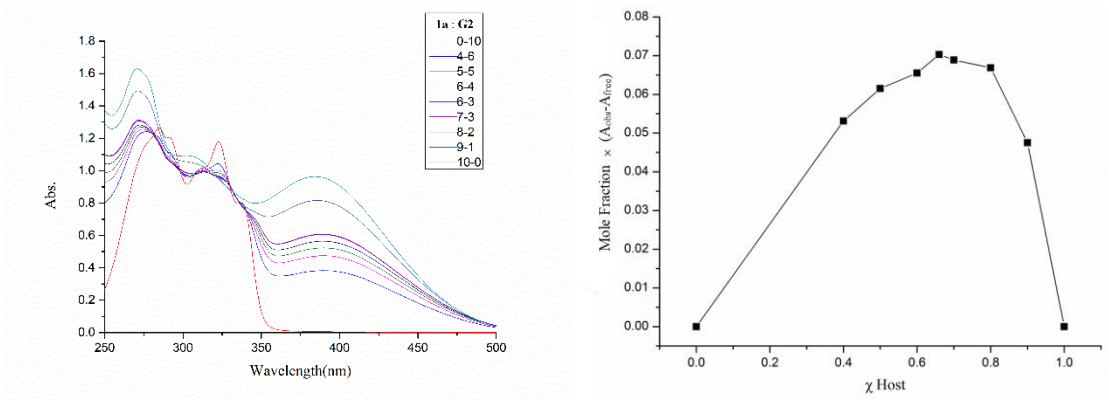


**Figure S42** Job plot analysis of the stoichiometric ratio between **1a** and **G2** in a solution of $CHCl_3/CH_3CN$ (1:1, v/v) at 298 K. The total concentration of **1a** and **G2** is held constant ([**1a**] + [**G2**] = 2.5 × $10^{-5}$ M. Absorbance intensity changes of **1a** recorded at 330 nm was used to analyze the binding ratio. The maximum on the Job plot lies at molar fraction around 0.67~0.71, pointing to the presence of both 4 : 2 and 5 : 2 H-G complexes.

## 4.5 Conformational Optimization of $\mathbf{1a_4 \supset G1_2}$ by xTB Method

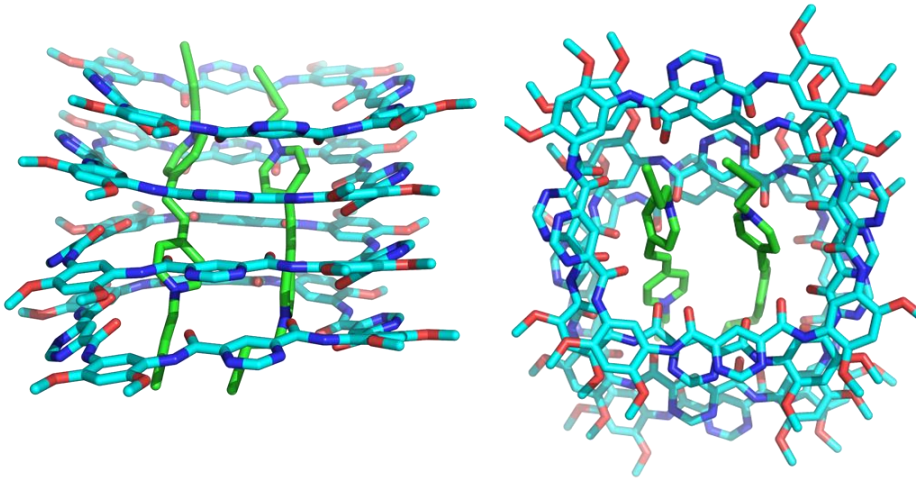

**Figure S43** Optimized superstructure of $\mathbf{1a_4 \supset G1_2}$ based on the semiempirical quantum–chemical calculations (xTB).

# 5. 2D NMR Spectra of [6]R

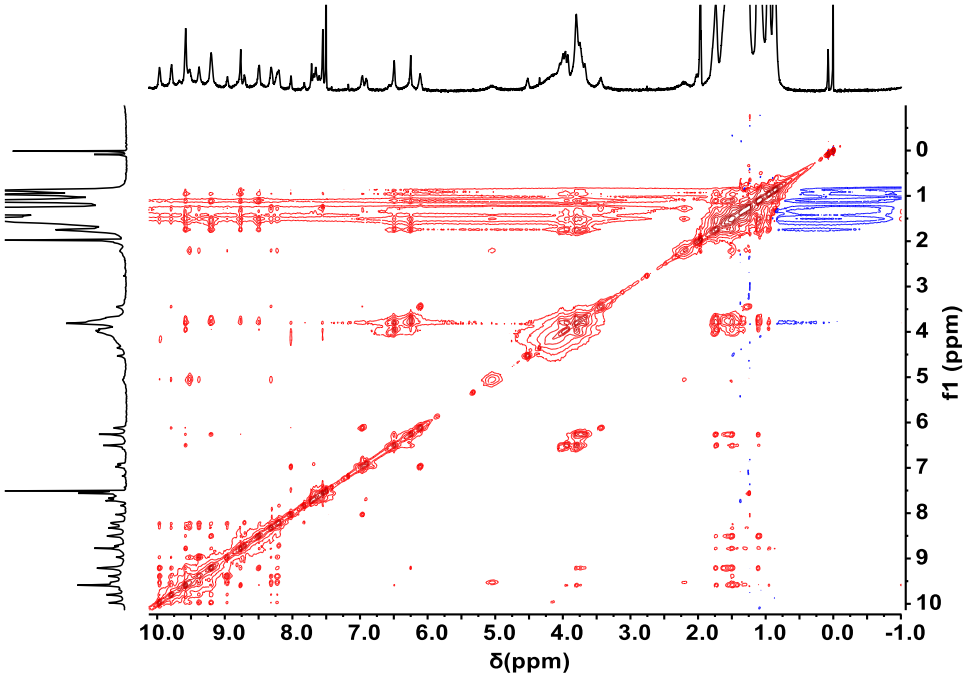


**Figure S44** 2D NOESY spectrum of **[6]Rs** (600 MHz, $CDCl_3/CD_3CN$, 1: 1, v/v, 298 K, 10 mM, mixing time = 0.4 s)

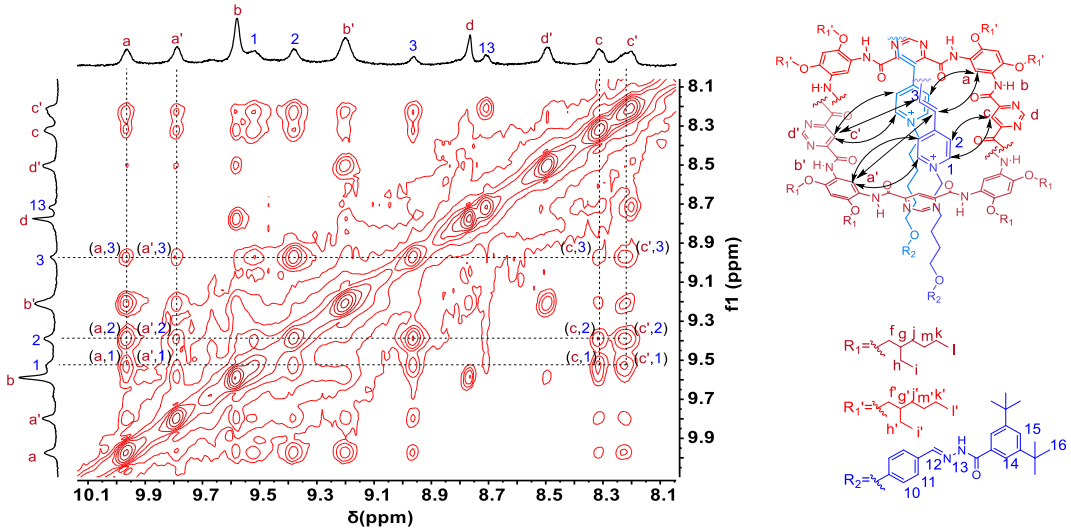


**Figure S45** Expanded 2D NOESY spectrum of **[6] Rs** (600 MHz, $CDCl_3/CD_3CN$, 1: 1, v/v, 298 K, 10 mM, mixing time = 0.4 s), indicating the interaction between **1a** and axle.

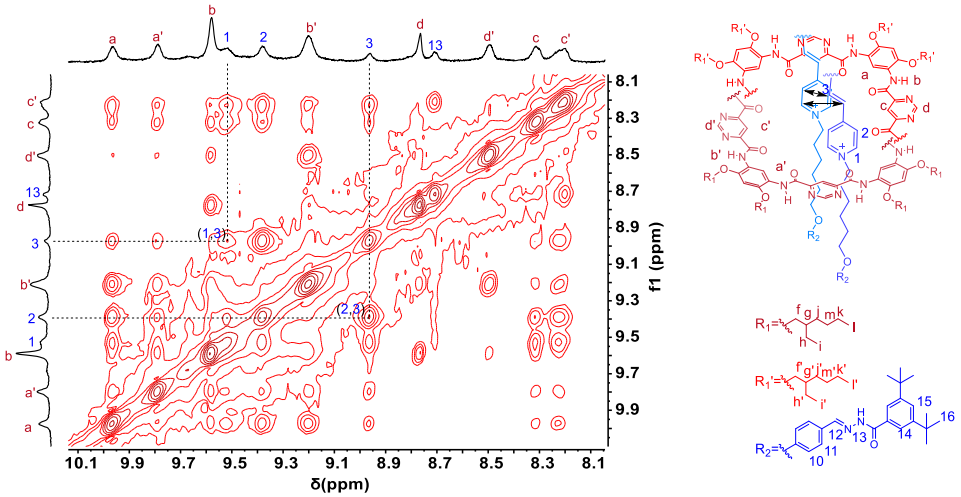


**Figure S46** Expanded 2D NOESY spectrum of **[6] Rs** (600 MHz, $CDCl_3/CD_3CN$, 1: 1, v/v, 298 K, 10 mM, mixing time = 0.4 s), indicating the interaction between two axles.

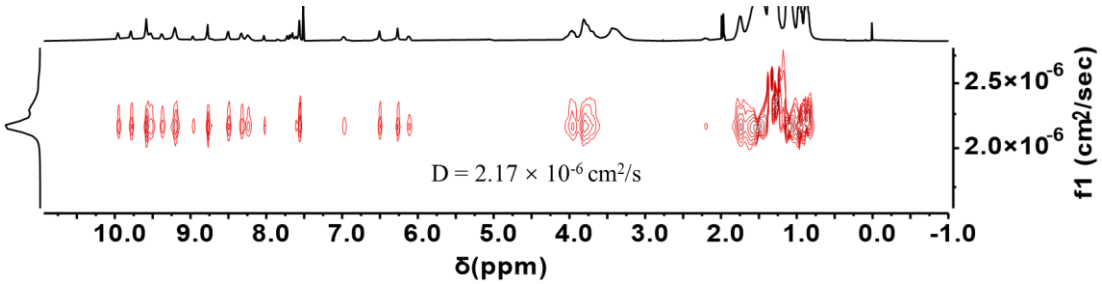


**Figure S47** $^1$H DOSY spectrum of **[6] Rs** (400 MHz, $CDCl_3/CD_3CN$, 1: 1, v/v, 298 K)

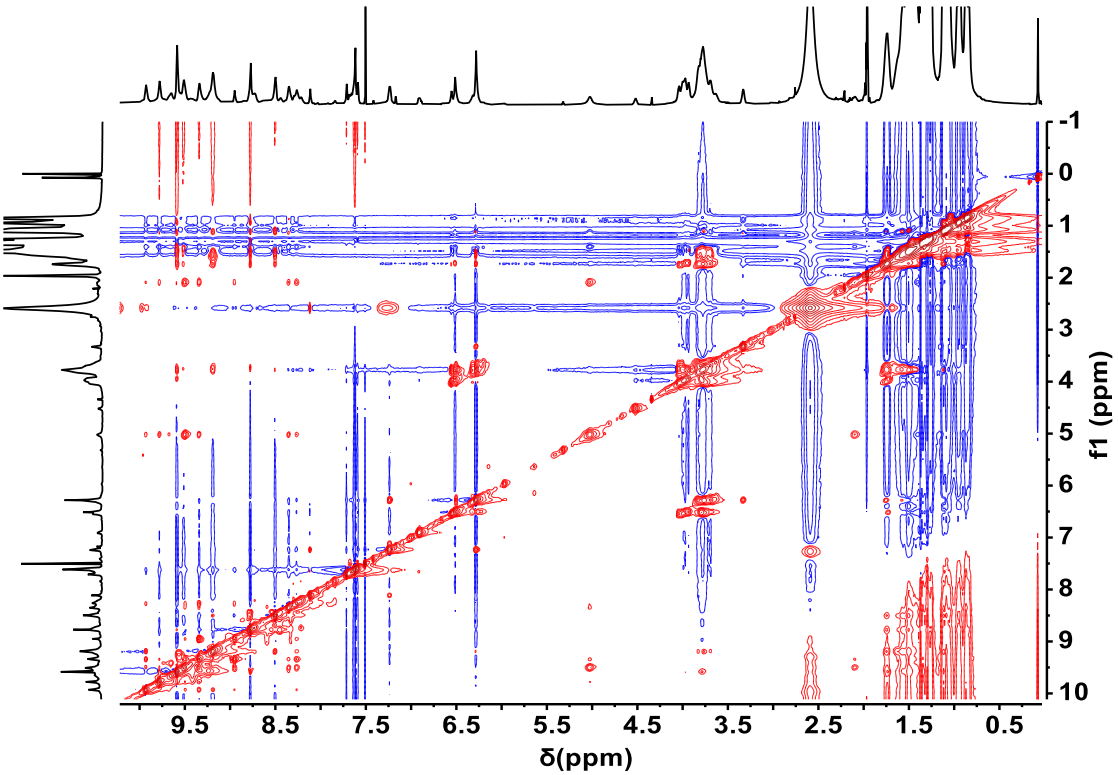


**Figure S48** 2D NOESY spectrum of **[6]Rc** (600 MHz, $CDCl_3/CD_3CN$, 1: 1, v/v, 298 K, 10 mM, mixing time = 0.4 s)

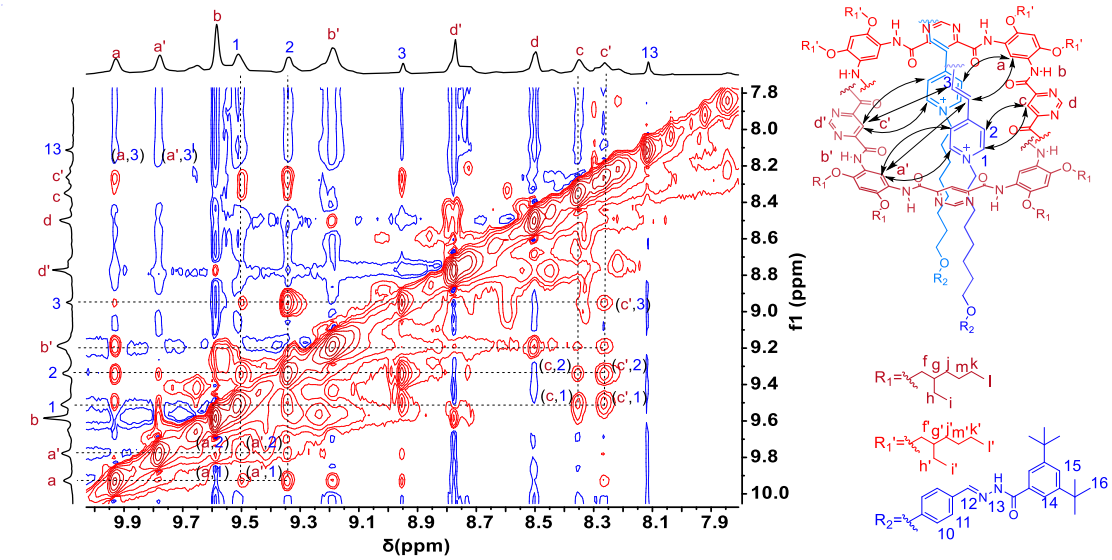


**Figure S49** Expanded 2D NOESY spectrum of **[6] Rs** (600 MHz, $CDCl_3/CD_3CN$, 1: 1, v/v, 298 K, 10 mM, mixing time = 0.4 s), indicating the interaction between **1a** and axle.

# 6. X-ray Single Crystal Structure

The crystal was grown in a slow solvent evaporation of $CHCl_3$ and $CH_3CN$ at 298K temperature with the red color and block shape. The single-crystal X-ray Diffraction measurement, which was carried out in a Rigaku Synergy X-ray Diffractometer equipped with hybrid pixel array detector and rotating-anode Cu X-ray source. The integration of the data set was performed by CrysAlisPro with $R_{int}$ = 0.065. The structure model was solved by SHELXT (version 2018/2) and refined by SHELXL (version 2019/2).

## 6.1 Crystal Parameters

**Table S2** Crystallographic data and structure refinement for **1a$_4$ ⊃ G1$_2$**

| **Identification code** | **1a$_4$ ⊃ G1$_2$** (CCDC **2324071**) |
|---|---|
| **Empirical formula** | $C_{246}H_{340}N_{34}O_{33}F_{12}P_2$ |
| **Formula weight** | 4591.44 |
| **Temperature/K** | 293(2) |
| **Crystal system** | triclinic |
| **Space group** | $P\bar{1}$ |
| **a/Å** | 21.5297(3) |
| **b/Å** | 24.7451(3) |
| **c/Å** | 29.6954(3) |
| **α/°** | 109.8680(10) |
| **β/°** | 104.1450(10) |
| **γ/°** | 101.3310(10) |

| | |
|---|---|
| **Volume/Å$^3$** | 13733.1(4) |
| **Z** | 2 |
| **$\rho_{calc}$g/cm$^3$** | 1.110 |
| **μ/mm$^{-1}$** | 0.757 |
| **F(000)** | 4912.0 |
| **Crystal size/mm$^3$** | 0.200 × 0.100 × 0.100 |
| **Radiation** | Cu Kα (λ = 1.54184) |
| **2Θ range for data collection/°** | 3.988 to 152.886 |
| **Index ranges** | -27 ≤ h ≤ 24, -31 ≤ k ≤ 31, -37 ≤ l ≤ 37 |
| **Reflections collected** | 196561 |
| **Independent reflections** | 55402 [$R_{int}$ = 0.0651, $R_{sigma}$ = 0.0660] |
| **Data/restraints/parameters** | 55402/1764/2250 |
| **Goodness-of-fit on F$^2$** | 2.226 |
| **Final R indexes [I>=2σ (I)]** | $R_1$ = 0.2457, $wR_2$ = 0.5642 |
| **Final R indexes [all data]** | $R_1$ = 0.3304, $wR_2$ = 0.6276 |
| **Largest diff. peak/hole / e Å$^{-3}$** | 1.94/-1.21 |

**Table S3** Containing the Check cif A alerts obtained from the checkcif.iucr.org webpage and the authors responses.

| Alerts level A | Author response |
|---|---|
| SHFSU01_ALERT_2_A The absolute value of parameter shift to su ratio > 0.20<br>Absolute value of the parameter shift to su ratio given 0.222<br>Additional refinement cycles may be required. | This is due to the highly disordered 2-ethylhexyl chains. |
| PLAT080_ALERT_2_A Maximum Shift/Error ..... 0.22 Why ? | This is due to the highly disordered 2-ethylhexyl chains. |
| PLAT082_ALERT_2_A High R1 Value ..... 0.25 Report | This is due to the highly disordered 2-ethylhexyl chains. |
| PLAT084_ALERT_3_A High wR2 Value (i.e. > 0.25) ..... 0.63 Report | This is due to the highly disordered 2-ethylhexyl chains. |
| PLAT201_ALERT_2_A Isotropic non-H Atoms in Main Residue(s) ..... 128 Report | This is due to the highly disordered 2-ethylhexyl chains. |
| PLAT411_ALERT_2_A Short Inter H...H Contact H8B_9 ..H8A_18 . 1.47 Ang. 1-x,1-y,1-z = 2_666 Check | This is due to the highly disordered 2-ethylhexyl chains. |
| PLAT411_ALERT_2_A Short Inter H...H Contact H4B_10 ..H8A_20 . 1.14 Ang. -1+x,-1+y,z = 1_445 Check | This is due to the highly disordered 2-ethylhexyl chains. |
| PLAT412_ALERT_2_A Short Intra XH3 .. XHn H9A_9 ..H9A_15 . 1.30 Ang. x,y,z = 1_555 Check | This is due to the highly disordered 2-ethylhexyl chains. |
| PLAT412_ALERT_2_A Short Intra XH3 .. XHn H5B_20 ..H6A_20 . 1.67 Ang. x,y,z = 1_555 Check | This is due to the highly disordered 2-ethylhexyl chains. |
| PLAT413_ALERT_2_A Short Inter XH3 .. XHn H9B_13 ..H9C_19 . 1.64 Ang. 1-x,2-y,1-z = 2_676 Check | This is due to the highly disordered 2-ethylhexyl chains. |
| PLAT413_ALERT_2_A Short Inter XH3 .. XHn H9B_16 ..H5A_21 . 1.89 Ang. x,1+y,z = 1_565 Check | This is due to the highly disordered 2-ethylhexyl chains. |
| PLAT934_ALERT_3_A Number of (Iobs-Icalc)/Sigma(W) > 10 Outliers .. 24 Check | This is due to the highly disordered 2-ethylhexyl chains. |

### 6.2 Quantification for the Stacking Distance between Two Macrocycles of 1a

Quantification is carried out according to literature methods.[1] The plane defined by 8 nitrogen atoms of pyrimidine in one macrocycle **1a** is selected as a reference plane. The distances from the 8 nitrogen atoms of pyrimidine in one adjacent macrocycle **1a** to the reference plane are measured.

The average value of the distance values is used as a quantitative value for the stacking distance between two adjacent H-bonded macrocycles.

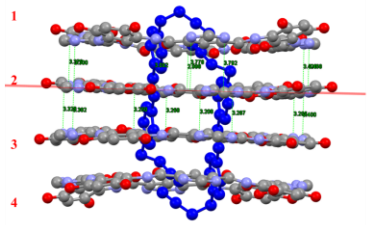


| Quantification for the stacking distance between two macrocycles of **1** | | |
|---|---|---|
| **macrocycles** | 1-2 | 3-2 |
| | 3.3 | 3.4 |
| | 3.4 | 3.3 |
| | 3.1 | 3.2 |
| | 3.0 | 3.3 |
| | 3.4 | 3.3 |
| | 3.4 | 3.4 |
| | 3.8 | 3.3 |
| | 3.8 | 3.2 |
| **average** | 3.4 | 3.3 |

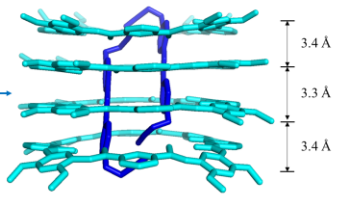


**Figure S50** Quantification for the stacking distance between two macrocycles of **1a**.

## 6.3 Quantification for the Conformation-Bending Degree of 1a

Quantification is carried out according to literature methods.[1] For a H-bonded macrocycle, the plane defined by 8 nitrogen atoms of pyrimidine acts as a reference plane. The dihedral angles between the reference plane and 8 aromatic rings are measured. The average value of these 8 dihedral angles is used as a quantitative value for the conformation-bending degree of H-bonded macrocycle.

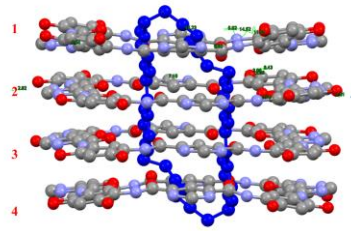


| Quantification for the conformation-bending degree of **1** (°) | | |
|---|---|---|
| **macrocycle** | 1(4) | 2(3) |
| **plane 1** | 14.5 | 3.0 |
| **plane 2** | 11.8 | 3.8 |
| **plane 3** | 15.2 | 7.1 |
| **plane 4** | 5.0 | 6.4 |
| **plane 5** | 23.0 | 12.0 |
| **plane 6** | 9.6 | 2.8 |
| **plane 7** | 16.6 | 0.8 |
| **plane 8** | 5.5 | 2.8 |
| **average** | 12.6 | 4.8 |

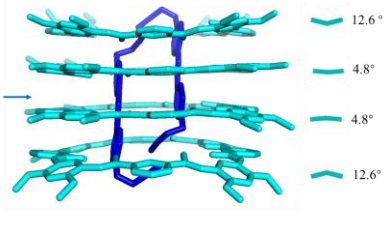


**Figure S51** Quantification for the conformation-bending degree of **1a**.

## 6.4 Measurement of Distance of Cation-Dipole Interactions

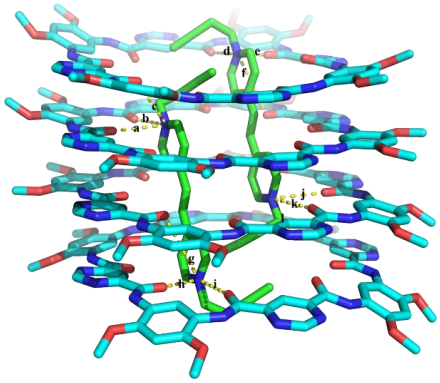


| No. of N⁺···O interaction | N⁺···O/Å |
|---|---|
| a | 3.1 |
| b | 4.0 |
| c | 3.6 |
| d | 4.1 |
| e | 3.0 |
| f | 4.3 |
| g | 4.3 |
| h | 3.0 |
| i | 4.1 |
| j | 3.1 |
| k | 4.0 |
| l | 3.6 |

**Figure S52** Measurement of distance of cation-dipole interactions. There are 12 cation-dipole interactions between O atoms on **1a** and $N^+$ on the nearby pyridinium on **G1** with a distance of 3.1~4.3 Å.

## 6.5 Measurement of Distance of C-H···π Interactions

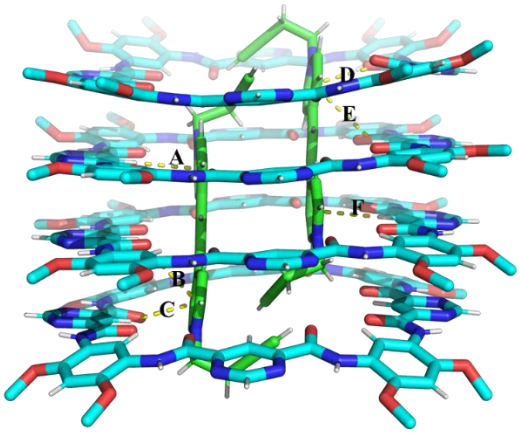


| No. of C-H···π interaction | C-H···π/Å |
|---|---|
| A | 3.0 |
| B | 4.0 |
| C | 3.1 |
| D | 3.1 |
| E | 4.0 |
| F | 3.0 |

**Figure S53** Measurement of distance of C-H···π interactions. There are 6 C-H···π interactions between hydrogens atoms on **1a** and the nearby pyridinium on **G1** with a distance of 3.0~4.0Å.

## 6.6 Measurement of Separation Distance and Calculation of Set-off Distance

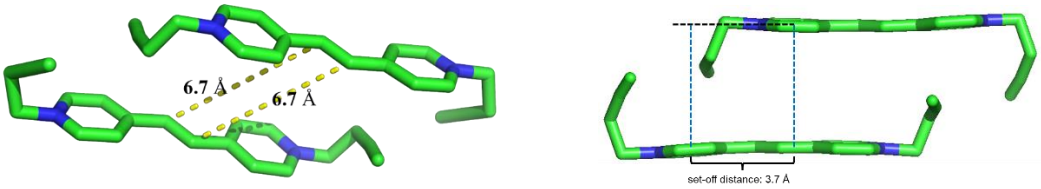


**Figure S54** Measurement of separation distance and calculation of set-off distance of two olefinic bonds. The two olefinic bonds are separated by 6.7 Å with an off-set distance of 3.7 Å. Hosts are hidden for clarity.

## 6.7 Atomic Displacement Parameters (ADPs) Drawings

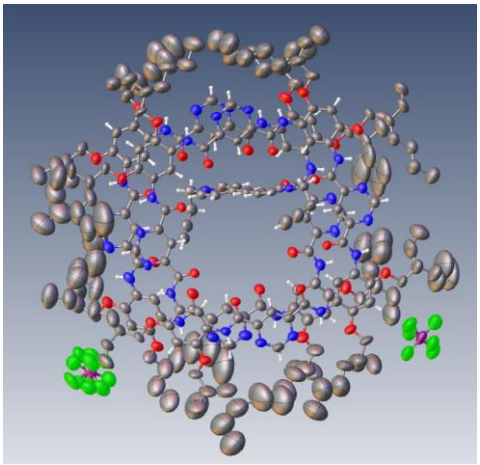

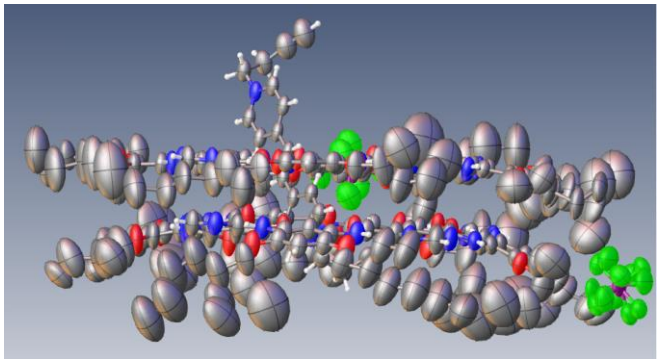

**Figure S55** Structural drawing showing atomic displacement parameters (ADPs) of each structure (top view and side view).

## 6.8 Measurement of Distance of Hydrogen Bonding Interactions

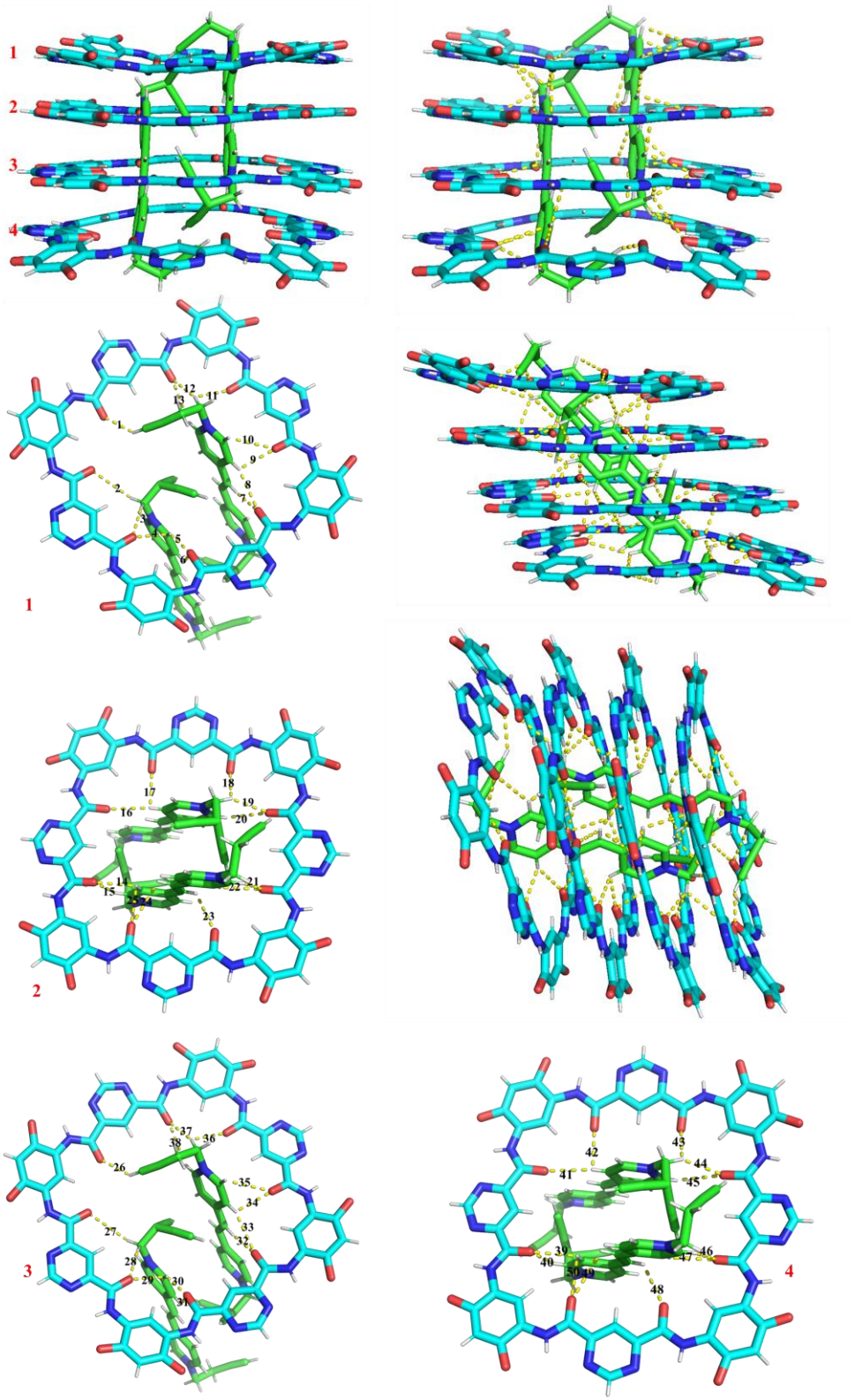


**Figure S56** Measurement of distance of hydrogen bonding interactions. There are 50 C-H···O interactions between oxygen atoms on **1a** and hydrogen atoms on **G1**, and H···O distance (Å) range from 2.3 to 3.1 and C-H···O angles (deg) range from 91.7 to 160.6.

**Table S4** C-H···O interactions between oxygen atoms on **1a** and hydrogen atoms on **G1**.

| No. of C-H···O interaction | H···O/Å C-H···O angles | No. of C-H···O interaction | H···O/Å C-H···O angles |
|---|---|---|---|
| **1** | **2.3 (137.8 °)** | **26** | **2.3 (137.8 °)** |
| **2** | **3.4 (123.3 °)** | **27** | **3.4 (123.3 °)** |
| **3** | **2.4 (150.6 °)** | **28** | **2.4 (150.6 °)** |
| **4** | **2.9 (112.5 °)** | **29** | **2.9 (112.5 °)** |
| **5** | **2.2 (136.1 °)** | **30** | **2.2 (136.1 °)** |
| **6** | **2.8 (109.8°)** | **31** | **2.8 (109.8°)** |
| **7** | **2.6(160.6 °)** | **32** | **2.6(160.6 °)** |
| **8** | **2.8 (150.5 °)** | **33** | **2.8 (150.5 °)** |
| **9** | **2.6 (107.3 °)** | **34** | **2.6 (107.3 °)** |
| **10** | **3.1 (91.7 °)** | **35** | **3.1 (91.7 °)** |
| **11** | **2.7 (102.0 °)** | **36** | **2.7 (102.0 °)** |
| **12** | **2.6 (161.7 °)** | **37** | **2.6 (161.7 °)** |
| **13** | **2.9 (145.3 °)** | **38** | **2.9 (145.3 °)** |
| **14** | **2.5 (115.7 °)** | **39** | **2.5 (115.7 °)** |
| **15** | **2.3 (127.2 °)** | **40** | **2.3 (127.2 °)** |
| **16** | **2.7 (163.9 °)** | **41** | **2.7 (163.9 °)** |
| **17** | **2.6 (93.7 °)** | **42** | **2.6 (93.7 °)** |
| **18** | **2.7(111.7 °)** | **43** | **2.7(111.7 °)** |
| **19** | **2.5 (148.8 °)** | **44** | **2.5 (148.8 °)** |
| **20** | **2.9 (145.0 °)** | **45** | **2.9 (145.0 °)** |
| **21** | **2.5(122.9°)** | **46** | **2.5(122.9°)** |
| **22** | **2.5 (121.5 °)** | **47** | **2.5 (121.5 °)** |
| **23** | **3.0(112.8 °)** | **48** | **3.0(112.8 °)** |
| **24** | **3.0 (109.3 °)** | **49** | **3.0 (109.3 °)** |
| **25** | **2.7 (103.0 °)** | **50** | **2.7 (103.0 °)** |

### 6.9 Visualization of Noncovalent Bonding Interactions

Independent gradient model (IGM) analysis is an approach[5] based on promolecular density (an electron density model prior to molecule formation) to identify and isolate intermolecular interactions. Crystal structures are used as input files. The binding surface was calculated by Multiwfn 3.8 program[6] and visualized using PyMOL[7]. In most cases, side chains are replaced by methyl groups. Strong polar attractions, van der Waals contacts and repulsive forces are visualized as an isosurface with blue, green and red color, respectively.

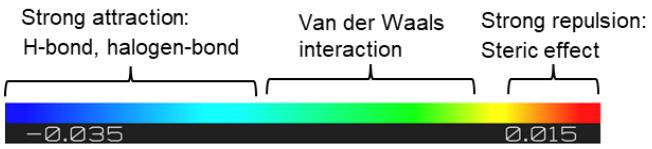


**Figure S57** Color-coded sign $(\lambda_2)_\rho$ scale bar.

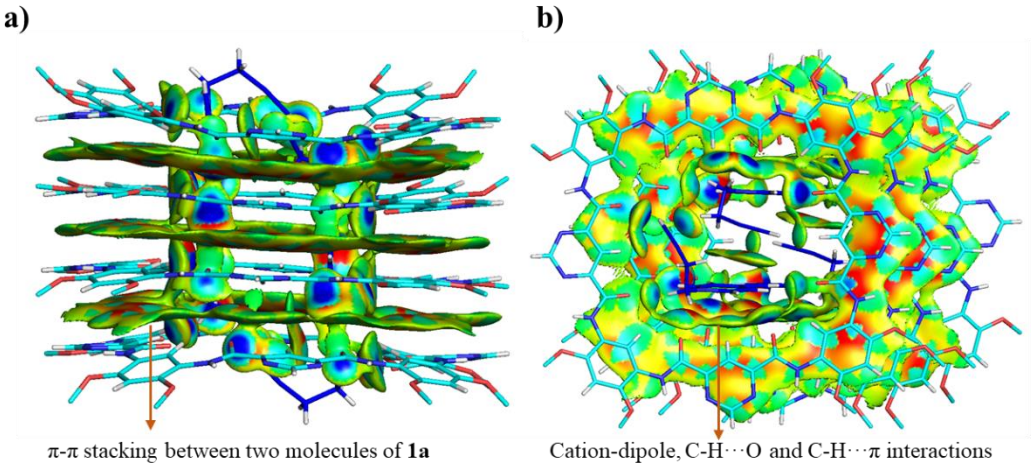


**Figure S58** Visualization of noncovalent bonding interactions in $\mathbf{1a_4} \supset \mathbf{G1_2}$.

## 6.10 Parallel Displaced π-π Stacking of 1a in Crystal Structure

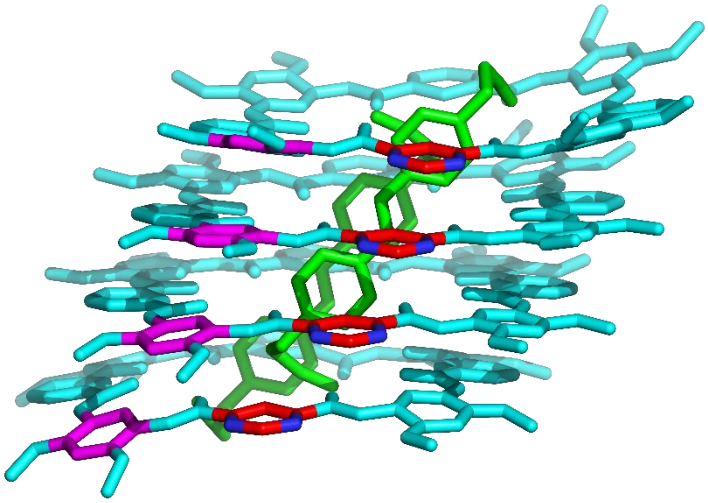

**Figure S59** The pyrimidium and phenyl subunits are devoid of any face-to-face π–π stacking interactions. Red for pyrimidium subunits and pink for phenyl subunits.

# 7. Stability of [6]R at Ambient and Elevated Temperature

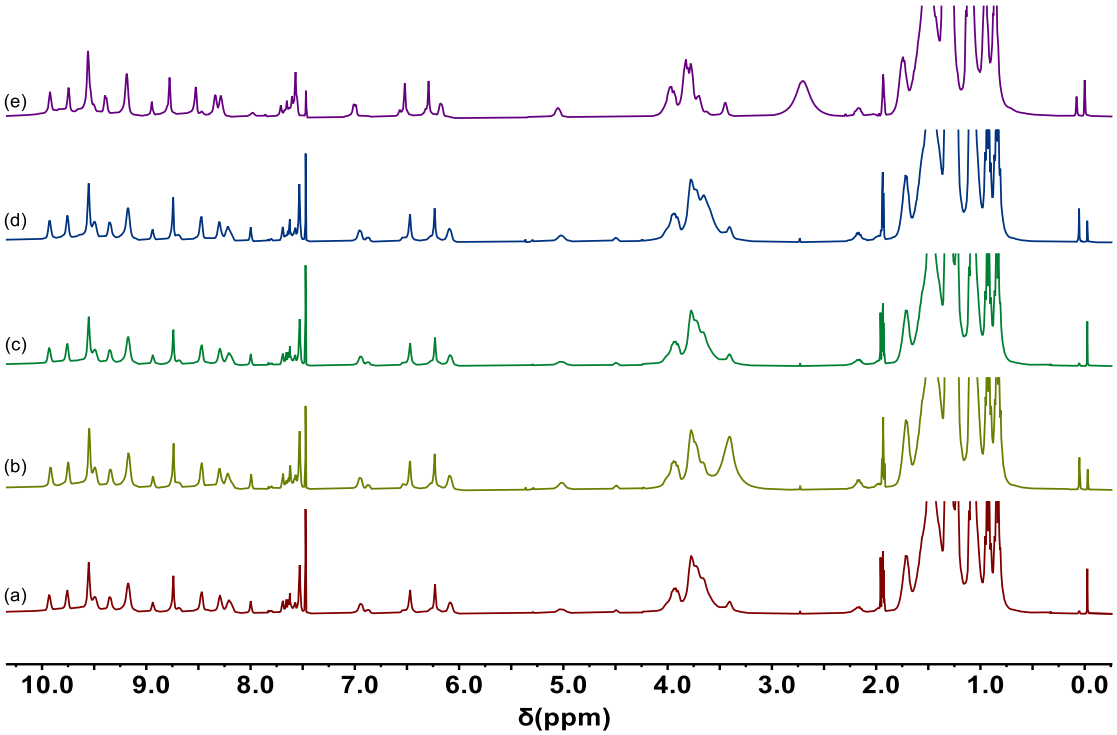


**Figure S60** $^{1}$H NMR spectra of (a) **[6]Rs**, (b) the same sample after 30 days at ambient temperature, (c) the same sample after 70 days at ambient temperature, (d) the same sample after heating at 60 ˚C for 48 h, (e) the same sample measured at 60 ˚C.

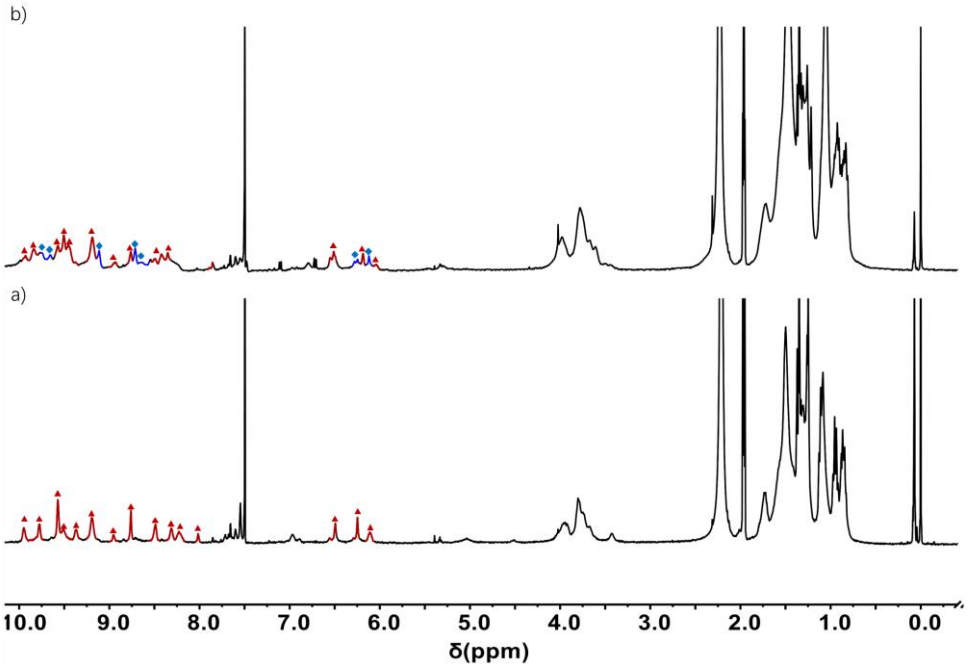


**Figure S61** $^{1}$H NMR of **[6]Rs** (4 Mm, bottom) and the mixture of **[6]Rs** (4 mM) and **1a** (1 mM) after heating at 60 ˚C for 48 h (top). (400 MHz, $CDCl_3/CD_3CN$,1 : 1, v/v, 298 K). Red triangle for **[6]Rs** and blue diamond for **1a**.

# 8. Confirming the Mechanically Interlocked Structure of [6]Rs by MS

The formation of interlocked structure is also evidenced by the mass experimental results of rotaxane **[6]Rs** and a 2:1 mixture of axle **Ax** and macrocycle **1a** (Fig. S62). The spectrum of **[6]Rs** (Fig. S62a) only shows a very intense signal at m/z = 2513.0819 that corresponds to the positive ion [**[6]Rs**-4$PF_6^-$]$^{4+}$, but no signal for the free axle **Ax** is observed. In contrast, strong signals for free positive ion [**Ax**-2$PF_6^-$]$^{2+}$ at m/z = 526.3462, free positive ion [**Ax**-$PF_6^-$]$^+$ at m/z = 1197.6500 and fragmented **Ax** at m/z = 617.3849 are obtained under the same conditions when a 2:1 mixture of axle **Ax** and macrocycle **1a** was tested (Fig. S62c). The absence of signal of rotaxane **[6]Rs** indicate that **1a** cannot threaded through the stoppered **Ax**. The absence of signal of **1a** may be caused by the ion suppression of ionic **Ax** since **1a** is electrically neutral. To further verify that the large ring (**1a**) cannot slip off at the ends of the axle without severing any covalent bonds, tandem MS experiments for the positive ion [**[6]Rs**-4$PF_6^-$]$^{4+}$ were performed. The **[6]Rs** was completely decomposed by fragmentation of the axle, resulting in the signals at m/z 1017.1844, 1347.3260 and 1519.9686 (Fig. S62b). These MS experimental results demonstrate that the large ring (**1a**) cannot slip off at the ends of the axle unless the axle is fragmented.

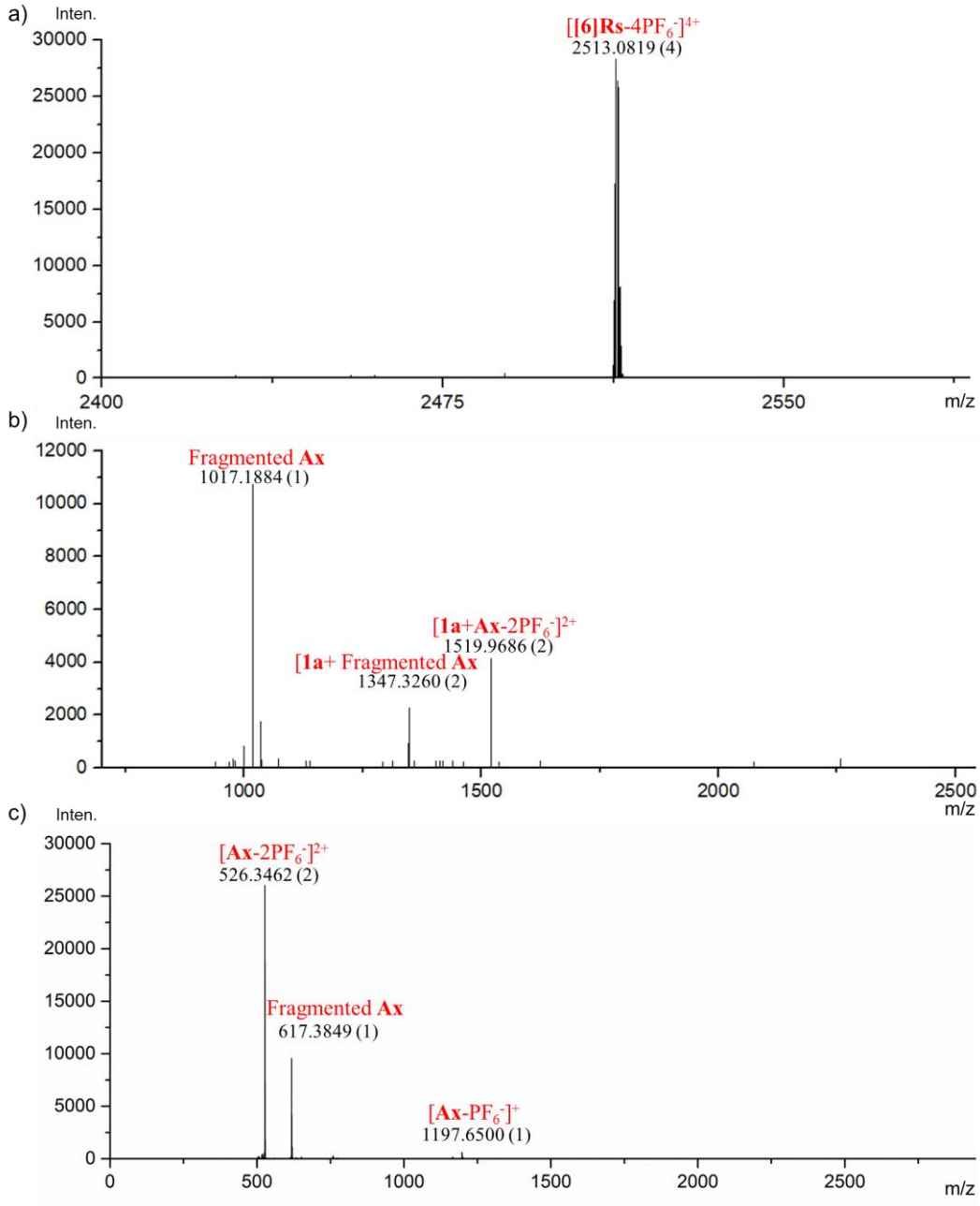


**Figure S62** a) ESI-HRMS spectrum of **[6]Rs**; b) ESI-MS/MS spectrum of **[6]Rs**; c) ESI-HRMS spectrum of the mixture of **Ax** and **1a**.

# 9. Conformational Optimization of [6]Rs by xTB Method

In order to gain a better understanding of the geometrical superstructure of **[6]Rs**, xTB calculations have been carried out based on the crystal structure of [6]pseudorotaxane. Figure S37 shows the energy minimized structure of **[6]Rs**.[8]

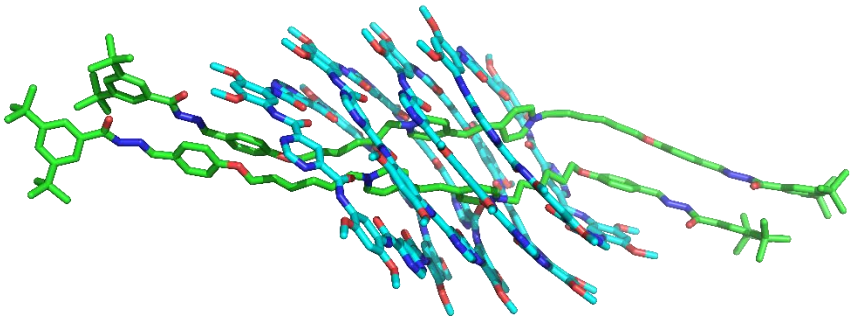

**Figure S63** Optimized superstructure of **[6]Rs**.

# References


[1] Z. Wang, L. Mei, C. Guo, S. Huang, W. Shi, X. Li, W. Feng, X. Li, C. Yang, and L. Yuan, *Angew. Chem. Int. Ed.*, 2023, **62**, e202216690.

[2] (a) T.-W. Wang, P.-R. Huang, J. Chow, W. Kaminsky and M. R. Golder, *J. Am. Chem. Soc.*, 2021, **143**, 7314-7319. (b) R. Zagami, G. Sortino, E. Caruso, M. C. Malacarne, S. Banfi, S. Patanè, L. M. Scolaro, and A. Mazzaglia, *Angew. Chem. Int. Ed.*, 2021, **60**, 1254-1262.

[3] X. Li, X. Yuan, P. Deng, L. Chen, Y. Ren, C. Wang, L. Wu, W. Feng, B. Gong and L. Yuan, *Chem. Sci*., 2017, **8**, 2091-2100.

[4] S. Cakmak, S. Fielden, U. Karaca, D. Leigh, C. Mcternan, D. Tetlow and M. Wilson, *Science*, 2017, **358**, 340-343.

[5] C. Lefebvre, G. Rubez, H. Khartabil, J.-C. Boisson, J. Contreras-García, E. Hénon, *Phys. Chem. Chem. Phys.* 2017, **19**, 17928-17936.

[6] T. Lu, F. Chen, *J. Comput. Chem.*, 2012, **33**, 580-592.

[7] The PyMOL Molecular Graphics System, Version 2.3.0 Schrödinger, LLC.

[8] J. Seibert, C. Bannwarth and S. Grimme, *J. Am. Chem. Soc*., 2017, **139**, 11682-11685.